miRNAs are generally down-regulated but sometimes up-regulated in cancers. In the present study, we found that the miR-27b level is decreased in breast cancerous tissues compared with noncancerous tissues. Immunohistochemical analyses revealed the high expression of CYP1B1 protein in breast cancerous tissues in accordance with previous studies (19, 34). The high expression of CYP1B1 protein in cancer cells would result from the decreased expression of miR-27b. The patients in the present study were both estrogen receptor–positive and progesterone receptor–positive. No association was observed between the levels of these receptors and the miR-27b or CYP1B1 level (data not shown). Furthermore, the miR-27b or CYP1B1 level was not associated with the presence or absence of lymph node metastasis (10 of 24 patients had lymph node metastasis). Thus, the biopathologic features or tumor stage of breast cancer would not affect the inverse association between the miR-27b and CYP1B1 levels. Highly expressed CYP1B1 in breast cancer would enhance the metabolism of 17β-estradiol. Whereas 17β-estradiol contributes to the growth and development of estrogen-dependent cancers, such as breast and endometrial cancers (16), 4-hydroxyestradiol formed by CYP1B1 causes DNA damage (17, 18). Thus, the abnormal expression of CYP1B1 would be related to the development of estrogen-dependent cancer.

More than half of the human miRNA genes are located at sites known to be involved in cancers, such as fragile sites, minimal regions of loss of heterozygosity, minimal regions of amplification, or common break point regions. Such locations support the notion that some miRNAs are involved in tumorigenesis. Calin et al. (35) reported that the gene coding miR-27b is located on the locus that is deleted in some cancers, such as urothelial or bladder cancer. It is plausible that the miR-27b would be down-regulated in these cancers. Human CYP1B1 is also expressed in urothelial and bladder tissues (36). The regulation of CYP1B1 by miR-27b would occur in these tissues, and the high CYP1B1 levels in urothelial or bladder cancer (36) might be due to the decreased miR-27b level.

The gene coding miR-27b is located on human 9q22.1, clustering with miR-23b and miR-24-1. Because these miRNAs are components of the same transcriptional unit (gi|4105182; ref. 37), the expression profiles of these miRNAs are considered to be in parallel. A moderate pairing with miR-24-1 is found at the neighborhood of MRE27b from +4,347 to +4,370 on the human *CYP1B1* gene, although the pairing probability is lower than that of miR-27b (miR-24-1, the score is 144 and the energy is −15.4 kcal/mol; miR-27b, the score is 158 and the energy is −29.5 kcal/mol; ref. 38).[4] miR-27a, which is a paralogous miRNA of miR-27b, has one nucleotide mismatch with the miR-27b and its pairing is possible (the score is 151 and the energy is −25.9 kcal/mol). Thus, the possibility that miR-24-1 or miR-27a may regulate the CYP1B1 expression cannot be excluded.

CYP1B1 is also expressed in eye tissue (39). Mutations or genetic polymorphisms of CYP1B1 are associated with primary congenital glaucoma (40, 41), and structural defect in eyes has been found in cyp1b1 knockout mice (42), indicating that CYP1B1 is responsible for eye development. At present, there is no information about the expression of miRNAs in eye tissue. The possibility that CYP1B1 level might be modulated by miR-27b in eye tissue in relation with eye development is worth pursuing in the future.

In conclusion, the results presented here suggested that human CYP1B1 is post-transcriptionally regulated by miR-27b, which would serve as a possible mechanism for the high expression of CYP1B1 protein in cancerous tissues. The silencing mechanism by miRNA might be one of the key factors regulating the cell-specific expression as well as individual differences in the expression of CYPs.

Acknowledgments

Received 4/17/2006; revised 6/15/2006; accepted 7/12/2006.

Grant support: Ministry of Health, Labor, and Welfare of Japan Research on Advanced Medical Technology, Health, and Labor Science Research grants and The Mochida Memorial Foundation for Medical and Pharmaceutical Research.

The costs of publication of this article were defrayed in part by the payment of page charges. This article must therefore be hereby marked *advertisement* in accordance with 18 U.S.C. Section 1734 solely to indicate this fact.

We thank Noriko Kawagishi (Futaba Breast Clinic, Kanazawa, Japan) for enthusiasm and research support and Brent Bell for reviewing the article.

[4] http://www.microrna.org.

References

1. Ambros V. The functions of animal microRNAs. Nature 2004;431:350–5.
2. Wienholds E, Plasterk RH. MicroRNA function in animal development. FEBS Lett 2005;579:5911–22.
3. Berezikov E, Guryev V, van de Belt J, Wienholds E, Plasterk R, Cuppen E. Phylogenetic shadowing and computational identification of human microRNA genes. Cell 2005;120:21–4.
4. Bartel DP. MicroRNAs: genomics, biogenesis, mechanism, and function. Cell 2004;116:281–97.
5. Lewis BP, Burge CB, Bartel DP. Conserved seed pairing, often flanked by adenosines, indicates that thousands of human genes are microRNA targets. Cell 2005;120:15–20.
6. Xie X, Lu J, Kulbokas EJ, et al. Systematic discovery of regulatory motifs in human promoters and 3′ UTRs by comparison of several mammals. Nature 2005;434:338–45.
7. Takamizawa J, Konishi H, Yanagisawa K, et al. Reduced expression of the *let-7* microRNAs in human lung cancers in association with shortened postoperative survival. Cancer Res 2004;64:3753–6.
8. Johnson SM, Grosshans H, Shingara J, et al. *RAS* is regulated by the *let-7* microRNA family. Cell 2005;120:635–47.
9. Calin GA, Dumitru CD, Shimizu M, et al. Frequent deletions and down-regulation of micro-RNA genes *miR15* and *miR16* at 13q14 in chronic lymphocytic leukemia. Proc Natl Acad Sci U S A 2002;99:15524–9.
10. Michael MZ, O' Connor SM, van Holst Pellekaan NG, Young GP, James RJ. Reduced accumulation of specific microRNAs in colorectal neoplasia. Mol Cancer Res 2003;1:882–91.
11. Sutter TR, Tang YM, Hayes CL, et al. Complete cDNA sequence of a human dioxin-inducible mRNA identifies a new gene subfamily of cytochrome P450 that maps to chromosome 2. J Biol Chem 1994;269:13092–9.
12. Shimada T, Hayes CL, Yamazaki H, et al. Activation of chemically diverse procarcinogens by human cytochrome P450 1B1. Cancer Res 1996;56:2979–84.
13. Hayes C, Spink D, Spink B, Cao J, Walker N, Sutter T. 17β-estradiol hydroxylation catalyzed by human cytochrome P450 1B1. Proc Natl Acad Sci U S A 1996;93:9776–81.
14. Spink D, Spink B, Cao J, et al. Induction of cytochrome P450 1B1 and catechol estrogen metabolism in ACHN human renal adenocarcinoma cells. J Steroid Biochem Mol Biol 1997;62:223–32.
15. Lee AJ, Cai MX, Thomas PE, Conney AH, Zhu BT. Characterization of the oxidative metabolites of 17β-estradiol and estrone formed by 15 selectively expressed human cytochrome P450 isoforms. Endocrinology 2003;144:3382–98.
16. Henderson IC, Canellos GP. Cancer of the breast: the past decade (first of two parts). N Engl J Med 1980;302:17–30.
17. Han X, Liehr JG. DNA single-strand breaks in kidneys of Syrian hamsters treated with steroidal estrogens: hormone-induced free radical damage preceding renal malignancy. Carcinogenesis 1994;15:997–1000.
18. Newbold RR, Liehr JG. Induction of uterine adenocarcinoma in CD-1 mice by catechol estrogens. Cancer Res 2000;60:235–7.
19. Murray GI, Taylor MC, McFadyen MCE, et al. Tumor-specific expression of cytochrome P450 CYP1B1. Cancer Res 1997;57:3026–31.
20. Cheung YL, Kerr AC, McFadyen MC, Melvin WT, Murray GI. Differential expression of CYP1A1, CYP1A2, CYP1B1 in human kidney tumours. Cancer Lett 1999;139:199–205.
21. Ragavan N, Hewitt R, Cooper LJ, et al. *CYP1B1* expression in prostate is higher in the peripheral than in the transition zone. Cancer Lett 2004;215:69–78.
22. Elston CW, Ellis IO. The value of histological grade in breast cancer: experience from a large study with long-term follow-up. Histopathology 1991;19:403–10.
23. Muskhelishvili L, Thompson PA, Kusewitt DF,

Wang C, Kadlubar FF. *In situ* hybridization and immunohistochemical analysis of cytochrome P450 1B1 expression in human normal tissues. J Histochem Cytochem 2001;49:229–36.
24. Griffiths-Jones S. The microRNA registry. Nucleic Acids Res 2004;32:D109–11.
25. Tsuchiya Y, Nakajima M, Yokoi T. Critical enhancer region to which AhR/ARNT and Sp1 bind in the human *CYP1B1* gene. J Biochem (Tokyo) 2003;133:583–92.
26. Tsuchiya Y, Nakajima M, Kyo S, Kanaya T, Inoue M, Yokoi T. Human *CYP1B1* is regulated by estradiol via estrogen receptor. Cancer Res 2004;64:3119–25.
27. Tsuchiya Y, Nakajima M, Takagi S, et al. Binding of steroidogenic factor-1 to the regulatory region might not critical for transcriptional regulation of human *CYP1B1* gene. J Biochem (Tokyo) 2006;139:527–34.
28. Shehin SE, Stephenson RO, Greenlee WF. Transcriptional regulation of the human *CYP1B1* gene. Evidence for involvement of an aryl hydrocarbon receptor response element in constitutive expression. J Biol Chem 2004;275:6770–6.
29. Zhang L, Savas U, Alexander DL, Jefcoate CR. Characterization of the mouse *Cyp1b1*: identification of an enhancer region that directs aryl hydrocarbon receptor-mediated constitutive and induced expression. J Biol Chem 1998;273:5174–83.
30. Zheng W, Jefcoate CR. Steroidogenic factor-1 interacts with cAMP response element-binding protein to mediate cAMP stimulation of *CYP1B1* via a far upstream enhancer. Mol Pharmacol 2005;67:499–512.
31. Lu J, Getz G, Miska EA, et al. MicroRNA expression profiles classify human cancers. Nature 2005;435:834–8.
32. Eis PS, Tam W, Sun L, et al. Accumulation of miR-155 and BIC RNA in human B cell lymphomas. Proc Natl Acad Sci U S A 2005;102:3627–32.
33. Chan JA, Krichevsky AM, Kosik KS. MicroRNA-21 is an antiapoptotic factor in human glioblastoma cells. Cancer Res 2005;65:6029–33.
34. McFadyen MC, Breeman S, Payne S, et al. J. Immunohistochemical localization of cytochrome P450 CYP1B1 in breast cancer with monoclonal antibodies specific for CYP1B1. J Histochem Cytochem 1999;47:1457–64.
35. Calin GA, Sevignani C, Dumitru CD, et al. Human microRNA genes are frequently located at fragile sites and genomic regions involved in cancers. Proc Natl Acad Sci U S A 2004;101:2999–3004.
36. Carnell DM, Smith RE, Daley FM, et al. Target validation of cytochrome P450 CYP1B1 in prostate carcinoma with protein expression in associated hyperplastic and premalignant tissue. Int J Radiat Oncol Biol Phys 2004;58:500–9.
37. Sempere LF, Freemantle S, Pitha-Rowe I, Moss E, Dmitrovsky E, Ambros V. Expression profiling of mammalian microRNAs uncovers a subset of brain-expressed microRNAs with possible roles in murine and human neuronal differentiation. Genome Biol 2004;5:R13.
38. John B, Enright AJ, Aravin A, Tuschl T, Sander C, Marks DS. Human microRNA targets. PLoS Biol 2004;2:e363.
39. Doshi M, Marcus C, Bejjani BA, Edward DP. Immunolocalization of CYP1B1 in normal, human, fetal, and adult eyes. Exp Eye Res 2006;82:24–32.
40. Stoilov I, Akarsu AN, Alozie I, et al. Sequence analysis and homology modeling suggest that primary congenital glaucoma on 2p21 results from mutations disrupting either the hinge region or the conserved core structures of cytochrome P4501B1. Am J Hum Genet 1998;62:573–84.
41. Bejjani BA, Stockton DW, Lewis RA, et al. Multiple CYP1B1 mutations and incomplete penetrance in an inbred population segregating primary congenital glaucoma suggest frequent *de novo* events and a dominant modifier locus. Hum Mol Genet 2000;9:367–74.
42. Libby RT, Smith RS, Savinova OV, et al. Modification of ocular defects in mouse developmental glaucoma models by tyrosinase. Science 2003;299:1578–81.

PHARMACOKINETICS, PHARMACODYNAMICS AND DRUG METABOLISM

Species Differences of Inhibitory Effects on P-Glycoprotein-Mediated Drug Transport

NAOTO SUZUYAMA,[1] MIKI KATOH,[1] TOSHIYUKI TAKEUCHI,[2] SUMIE YOSHITOMI,[2] TOMOAKI HIGUCHI,[2] SATORU ASASHI,[2] TSUYOSHI YOKOI[1]

[1]Drug Metabolism and Toxicology, Division of Pharmaceutical Sciences, Graduate School of Medical Science, Kanazawa University, Kakuma-machi, Kanazawa 920-1192, Japan

[2]Development Research Center and Discovery Research Center, Pharmaceutical Research Division, Takeda Pharmaceutical Company Limited, Osaka, Japan

Received 5 June 2006; revised 15 August 2006; accepted 27 August 2006

Published online in Wiley InterScience (www.interscience.wiley.com). DOI 10.1002/jps.20787

ABSTRACT: Previously, we clarified the species differences in P-glycoprotein (P-gp)-mediated drug transport activity using human *MDR1*, monkey *MDR1*, canine *MDR1*, rat *MDR1a*, rat *MDR1b*, mouse *mdr1a*, and mouse *mdr1b* transfected LLC-PK_1 cell lines. However, the species differences in the inhibitory effects on P-gp-mediated drug transport have not been clarified yet. The purpose of the present study was to evaluate the species differences in the inhibitory effects of typical P-gp inhibitors, quinidine and verapamil, on P-gp-mediated drug transport using *MDR1* transfected cell lines. The transcellular transport of [^{3}H]daunorubicin, [^{3}H]digoxin, and [*mebmt*-β-^{3}H]cyclosporin A across monolayers of the *MDR1* transfected cells were measured in the presence or absence of P-gp inhibitors. On daunorubicin transport, the relative IC_{50} value (quinidine IC_{50}/verapamil IC_{50}) of human P-gp was 5.25 and those from other species ranged from 0.89 to 10.70. The transport of digoxin and cyclosporin A also showed different relative IC_{50} values among human, monkey, canine, rat, and mouse P-gps. The present study revealed that species differences in the inhibitory effects on P-gp-mediated drug transport should not be disregarded among human, monkey, canine, rat, and mouse. This study will provide useful information for predicting drug interactions mediated by P-gp. © 2006 Wiley-Liss, Inc. and the American Pharmacists Association J Pharm Sci 96:1609–1618, 2007

Keywords: multidrug resistance transporters; P-glycoprotein; inhibition; species differences; drug interaction; drug transporter

INTRODUCTION

P-glycoprotein (P-gp) encoded by *multidrug resistance 1* (*MDR1*) was found to be an energy-dependent efflux transporter driven by ATP hydrolysis in Chinese hamster ovary cell mutants.[1–3] P-gp is localized in the apical membrane of cells[4] and can transport a variety of compounds including drugs. Since P-gp exhibits broad substrate specificity, P-gp expressing cells show cross-resistance to diverse drugs. In addition, since P-gp is expressed not only in tumor cells but in normal tissue such as intestine, liver, kidney, placenta, testis, and in the capillary endothelial cells of brain,[5] it plays an important

Correspondence to: Tsuyoshi Yokoi (Telephone: +81-76-234-4407; Fax: +81-76-234-4407; E-mail: TYOKOI@kenroku.kanazawa-u.ac.jp)

Journal of Pharmaceutical Sciences, Vol. 96, 1609–1618 (2007)

role in the absorption, distribution, and excretion of drugs.

Due to its localization, P-gp has a great impact on limiting the cellular uptake of an oral drug from the intestinal lumen into the epithelium and from blood into the brain. Many drug interactions via P-gp have been reported. The coadministration of a P-gp inhibitor can lead to a change in the disposition of a P-gp substrate, resulting in an increase of the oral bioavailability, a decrease of the elimination, and the occurrence of adverse effects.[6–8] Therefore, it is essential to investigate whether a drug candidate interacts with P-gp and whether its pharmacokinetic behavior can be influenced by P-gp inhibitors. Previously, we revealed species differences in P-gp-mediated drug transport activity[9] using the *MDR1* transfected cell lines, in which the cDNA was from human, monkey, canine, rat, and mouse.[10] However, species differences in the inhibitory effects on P-gp-mediated drug transport are still unclear. The purpose of the present study is to evaluate the species differences in the inhibitory effects on P-gp-mediated daunorubicin, digoxin, and cyclosporin A transport by typical P-gp inhibitors, quinidine and verapamil.

MATERIALS AND METHODS

Materials

[^{3}H]Daunorubicin (303.4 or 592.0 GBq/mmol) and [^{3}H]digoxin (358.4 GBq/mmol) were purchased from PerkinElmer Life Sciences (Boston, MA). [*mebmt*-β-^{3}H]Cyclosporin A (296.0 GBq/mmol) was obtained from Amersham Biosciences (Buckinghamshire, UK). Colchicine, quinidine sulfate dihydrate, and verapamil hydrochloride were purchased from Wako Pure Chemical Industries (Osaka, Japan). All other materials were of the highest purity available.

Cell Culture

The *MDR1* transfected cell lines designated as hMDR1 (human *MDR1*), pMDR1 (monkey *MDR1*), cMDR1 (canine *MDR1*), rMDR1a (rat *MDR1a*), rMDR1b (rat *MDR1b*), mmdr1a (mouse *mdr1a*), and mmdr1b (mouse *mdr1b*), in which each *MDR1* cDNA transfected into LLC-PK$_1$ cells and a mock cell line were established by Takeuchi et al.[10] The mock cell line was transfected with an empty vector into LLC-PK$_1$ cells. The *MDR1* transfected cells were incubated in complete medium consisting of Medium 199 (Nissui Pharmaceutical, Tokyo, Japan) with 10% fetal bovine serum (Trace Scientific, Melbourne, Australia), 500 μg/mL G418 (MP Biomedicals, Irvine, CA), and 150 ng/mL of colchicine. For mock cells, colchicine was removed from the medium used for the *MDR1* transfected cells. The cells were cultured in an atmosphere of 5% CO_2-95% air at 37°C.

Inhibition of Transcellular Transport

The measurement of the transcellular transport was performed according to a procedure described previously.[9] The *MDR1* transfected cells and mock cells were seeded on microporous polycarbonate membrane filters (Transwell™, 3402, Corning, Acton, MA) at a cell density of 7.5×10^5 cells/cm^2. Cells were cultured on the membrane filter with 1.5 and 0.5 mL of complete medium in the outside and inside of the chamber, respectively, in an atmosphere of 5% CO_2-95% air at 37°C for 4 days. Fresh medium was replaced on the second day and the fresh medium without G418 and colchicine was replaced on the third day after seeding. Three hours before the start of the experiments, all culture media were replaced with fresh medium with neither G418 nor colchicine. Then the transepithelial electrical resistance (TEER) values across the cell monolayers were measured using the Millicell®-ERS (Millipore, Billerica, MA). The well in which the TEER value showed 80 Ω or greater after subtracting the resistance obtained in the control blank well was used for the experiment of the transcellular transport. The transport activities were almost the same in wells exhibiting more than 80 ohm/cm^2 of TEER. To examine the inhibitory effects of quinidine and verapamil on P-gp-mediated drug transport in the *MDR1* transfected cells and mock cells, inhibitors were added into the medium on both sides of the cell monolayers 1 h before adding the substrate. The medium on the donor side of the monolayers was added with 25.8 nM [^{3}H]daunorubicin (7.8 and 15.3 kBq/mL), 15.2 nM [^{3}H]digoxin (5.4 kBq/mL), or 30.7 nM [*mebmt*-β-^{3}H]cyclosporin A (9.1 kBq/mL) and the monolayers were then incubated in 5% CO_2-95% air at 37°C. Aliquots from the receiver side (50 μL of inside or 150 μL of outside) were taken at 3 h. The radioactivity was measured using a liquid scintillation counter (LSC 5100, Aloka, Tokyo, Japan) after the addition of 4 mL scintillation cocktail, Clear-sol I (Nacalai

DOI 10.1002/jps

tesque, Kyoto, Japan). In the *MDR1* transfected cells and mock cells, the transcellular transports of all P-gp substrates in our experimental conditions appeared to be almost linear up to 3 h after the start of the experiment.

For the intracellular accumulation study, the cells were washed thoroughly with ice-cold phosphate-buffered saline immediately after sampling. The cells were solubilized with 0.5 mL of 0.3 M NaOH overnight and were neutralized with 0.5 mL of 0.3 M HCl. The radioactivity of a 200 μL portion of the aliquots was measured. The protein contents of the *MDR1* transfected cells and mock cells were measured using the method of Lowry et al.[11]

The net transport was calculated by subtracting the apical-to-basolateral transport from the basolateral-to-apical transport at 3 h. To obtain the 50%-inhibitory concentration (IC_{50}), the concentrations of quinidine were as follows.

Daunorubicin transport: 0, 10, 20, 50, and 100 μM; digoxin transport: 0, 10, 20, and 50 μM; cyclosporin A transport: 0, 10, 20, and 50 μM (hMDR1, cMDR1, rMDR1b, and mmdr1b) or 0, 5, 10, 20, and 50 μM (pMDR1, rMDR1a, and mmdr1a).

The concentrations of another inhibitor, verapamil, were as follows. Daunorubicin transport: 0, 2, 10, 20, and 50 μM; digoxin transport: 0, 10, 20, and 50 μM (hMDR1, pMDR1, cMDR1, rMDR1a, and mmdr1a) or 0, 5, 10, 20, and 50 μM (rMDR1b and mmdr1b); cyclosporin A transport: 0, 10, 30, and 50 μM (hMDR1, pMDR1, rMDR1a, rMDR1b, and mmdr1a) or 0, 1, 10, 30, and 50 μM (mmdr1b).

In this study, the P-gp substrates and inhibitors showed no cell cytotoxicity in our experimental conditions. The data were calculated by using three or more independent measurements.

RESULTS

Effect of Quinidine and Verapamil on P-gp-Mediated Drug Transport in *MDR1* Transfected Cells and Mock Cells

The transcellular transports of daunorubicin in the presence of quinidine and verapamil, which are known as P-gp inhibitors, are shown in Figures 1 and 2. In the *MDR1* transfected cells, the basolateral-to-apical transport of daunorubicin was decreased, while the apical-to-basolateral transport was increased by quinidine and verapamil in a concentration-dependent manner. On the other hand, in the mock cells, the transcellular transport of daunorubicin did not change in the presence of inhibitors.

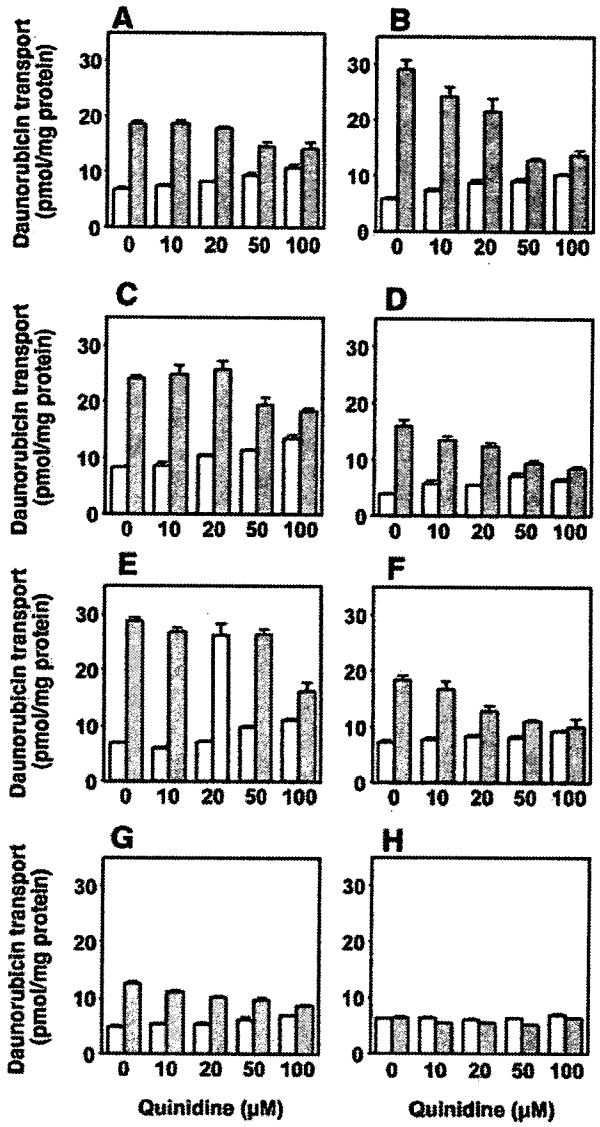

Figure 1. Concentration-dependent effect of quinidine on the transcellular transport of daunorubicin across the monolayers of *MDR1* transfected cells (A–G) and mock cells (H) at 3 h. (A) hMDR1. (B) pMDR1. (C) cMDR1. (D) rMDR1a. (E) rMDR1b. (F) mmdr1a. (G) mmdr1b. (H) mock. Open bar, daunorubicin was added to the medium of the apical side; shaded bar, daunorubicin was added to the medium of the basolateral side. The concentration of daunorubicin was 25.8 nM. Each column represents the mean ± SEM of three or more independent measurements.

To evaluate the species differences in the inhibitory effect on the net transport of daunorubicin

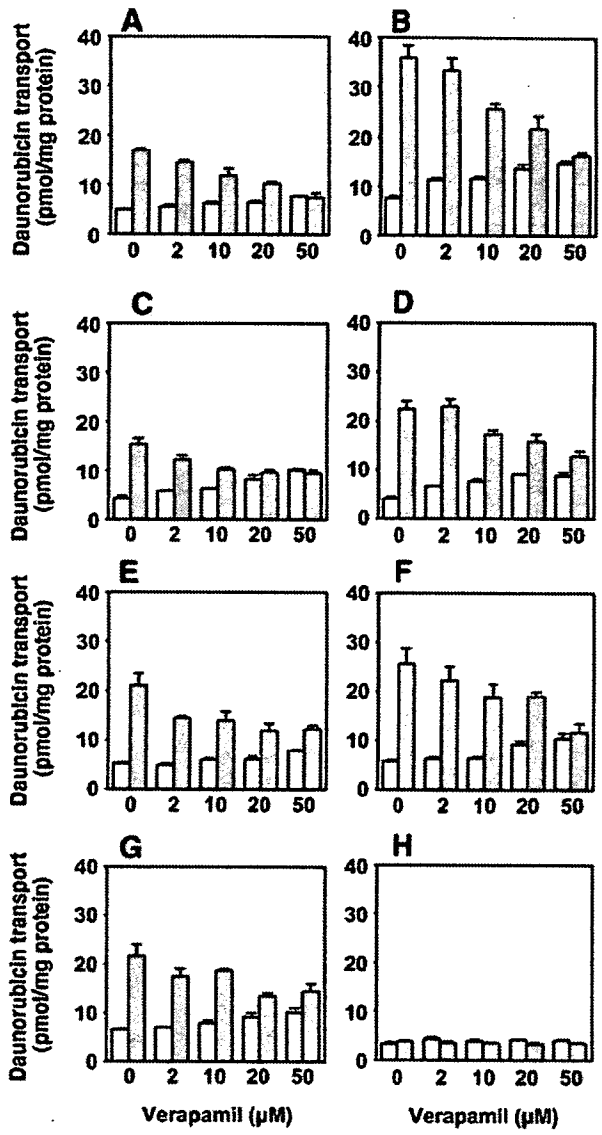

Figure 2. Concentration-dependent effect of verapamil on the transcellular transport of daunorubicin across the monolayers of *MDR1* transfected cells (A–G) and mock cells (H) at 3 h. (A) hMDR1. (B) pMDR1. (C) cMDR1. (D) rMDR1a. (E) rMDR1b. (F) mmdr1a. (G) mmdr1b. (H) mock. Open bar, daunorubicin was added to the medium of the apical side; shaded bar, daunorubicin was added to the medium of the basolateral side. The concentration of daunorubicin was 25.8 nM. Each column represents the mean ± SEM of three or more independent measurements.

via P-gp, the apparent IC_{50} values of quinidine and verapamil were determined. The net transports of daunorubicin in the presence of the inhibitors are shown in Figure 3. The IC_{50} values of quinidine and verapamil are summarized in Table 1. In the case of quinidine, the IC_{50} value of hMDR1 was 46.7 μM, which was similar to that of cMDR1 and mmdr1b. In the case of verapamil, the IC_{50} value of hMDR1 was 8.9 μM, which was similar to that of pMDR1, rMDR1a, and rMDR1b. The relative IC_{50} value (quinidine IC_{50}/verapamil IC_{50}) of hMDR1 was 5.25 and those of the other *MDR1* transfected cells ranged from 0.89 (mmdr1a) to 10.70 (cMDR1).

To investigate the species differences in the inhibitory effect using other P-gp substrates, the IC_{50} values of quinidine and verapamil for the digoxin and cyclosporin A transport were determined (Table 1). The net transports of digoxin and cyclosporin A in the presence of the inhibitors are shown in Figures 4 and 5, respectively. The residual net transports of digoxin in the presence of 50 μM quinidine in pMDR1, rMDR1b, and mmdr1b and that of cyclosporin A in the presence of 50 μM verapamil in cMDR1 were more than 50%, thus the concentration-dependent inhibitions were not investigated. For the digoxin transport, the IC_{50} value of quinidine in hMDR1 was 18.3 μM, which was almost the same as those of cMDR1 and mmdr1a (Table 1). On the other hand, the IC_{50} values of verapamil in pMDR1 and rMDR1a were similar to that of hMDR1. The relative IC_{50} value of hMDR1 was 1.00 and those of the other *MDR1* transfected cells ranged from 0.50 (cMDR1) to up to 6.17 (mmdr1b). For the cyclosporin A transport, the IC_{50} value of quinidine in hMDR1 was 21.9 μM, which was similar to that of rMDR1b (Table 1). The IC_{50} value of verapamil in hMDR1 was 44.4 μM, which was similar to those of rMDR1a and mmdr1a. The relative IC_{50} value of hMDR1 was 0.49 and those of other *MDR1* transfected cells ranged from 0.15 (rMDR1) to 3.30 (mmdr1b).

Intracellular Accumulation

The intracellular accumulation in daunorubicin transport at 3 h in the presence or absence of P-gp inhibitors in hMDR1 and mock cells is shown in Figure 6. The intracellular accumulation of the apical-to-basolateral and the basolateral-to-apical transport in hMDR1 was increased by quinidine and verapamil in a concentration-dependent manner. As in hMDR1, the intracellular accumulation in the other *MDR1* transfected cells also showed an increase in the presence of the inhibitors (data not shown). On the other hand, in mock cells, there was no difference in the

DOI 10.1002/jps

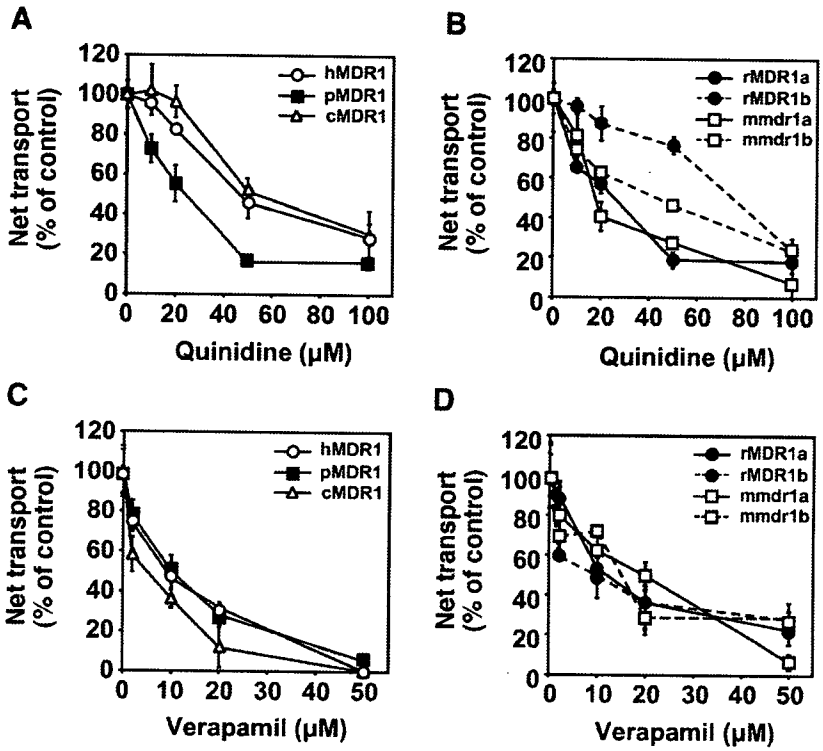

Figure 3. Concentration-dependent inhibition of the net transport of daunorubicin by quinidine (A and B) and verapamil (C and D) at 3 h in *MDR1* transfected cells. (B and D) A solid line shows the MDR (mdr) 1a. A dotted line shows MDR (mdr) 1b. The concentration of daunorubicin was 25.8 nM. Each point represents the mean ± SEM of three or more independent measurements.

intracellular accumulation by quinidine and verapamil. For the digoxin transport, the intracellular accumulation in the apical-to-basolateral and the basolateral-to-apical transport showed no increase in both the *MDR1* transfected cells and mock cells by quinidine and verapamil (data not shown). In the case of cyclosporin A, the intracellular accumulation in the *MDR1* transfected cells and mock cells was similar to the daunorubicin accumulation (data not shown).

Table 1. The IC_{50} Values of Quinidine and Verapamil on the Net Transport of Daunorubicin, Digoxin, and Cyclosporin A in *MDR1* Transfected Cells

	Daunorubicin		Digoxin		Cyclosporine A	
	Quinidine	Verapamil	Quinidine	Verapamil	Quinidine	Verapamil
hMDR1	46.7	8.9	18.3	18.3	21.9	44.4
pMDR1	24.1	10.0	>50.0	17.3	7.5	21.6
cMDR1	53.5	5.0	25.0	47.6	35.1	>50.0
rMDR1a	25.3	11.9	32.3	13.9	6.0	38.8
rMDR1b	75.0	12.5	>50.0	8.7	19.9	26.4
mmdr1a	17.6	19.7	22.7	38.3	10.7	49.6
mmdr1b	43.1	15.0	>50.0	8.1	30.4	9.2

The concentrations of daunorubicin, digoxin, and cyclosporine A were 25.8, 15.2, and 30.7 nM, respectively. For daunorubicin transport, the concentration of quinidine and verapamil ranged from 0 to 100 μM and from 0 to 50 μM, respectively. For digoxin and cyclosporin A transports, the concentration of quinidine and verapamil ranged from 0 to 50 μM.

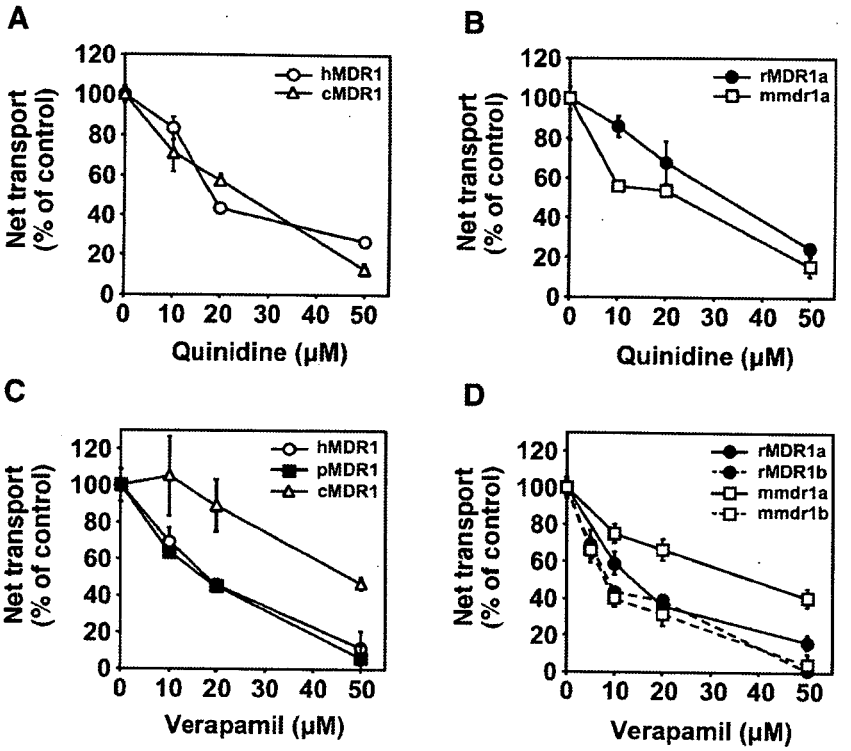

Figure 4. Concentration-dependent inhibition of the net transport of digoxin by quinidine (A and B) and verapamil (C and D) at 3 h in *MDR1* transfected cells. (B and D) A solid line shows the MDR (mdr) 1a. A dotted line shows MDR (mdr) 1b. The concentration of digoxin was 15.2 nM. Each point represents the mean ± SEM of three or more independent measurements.

DISCUSSION

It is increasingly recognized that drug transporters as well as drug metabolizing enzymes also play important roles in drug absorption, distribution, and excretion. The functions of the transporter proteins have been characterized by *in vitro* and *in vivo* experiments using tumor cells, transporter protein overexpressing cells, or gene-knockout animals.[8] The efflux drug transporter P-gp is the best studied among ATP-binding cassette drug efflux transporters to date. P-gp was clarified to play key roles in the drug absorption, disposition, and excretion in *in vitro* and *in vivo* studies.[12,13] The knowledge of the species differences in the function of P-gp would be helpful to extrapolate the pharmacokinetics from experimental animals to humans. Recently, we clarified that there were the species differences in the transport activity of P-gp by using hMDR1, pMDR1, cMDR1, rMDR1a, rMDR1b, mmdr1a, and mmdr1b cells.[9] The inhibition of P-gp activity as a cause of drug interactions has been reported in animals and humans.[6,14,15] However, there was almost no information about the species differences in the inhibitory effects on the P-gp function. In the present study, we investigated the species differences in the inhibitory effects by typical P-gp inhibitors, quinidine and verapamil, on the P-gp-mediated drug transport.

The *MDR1* transfected cells and mock cells used in this study were the same cell strains in the same culture conditions that were compared by our previous study,[9] and the P-gp expression level in the present study was the same as in that study. Therefore, stable expression level of P-gp in this study was thought to be the same as in our previous study.

First, the inhibitory effects on daunorubicin transport were determined. All *MDR1* transfected cells used in the present study except for mmdr1a exhibited much more potent inhibition by verapamil than by quinidine. For hMDR1, the present result was consistent with a previous report by Cardarelli et al.[16] in which verapamil was found to

DOI 10.1002/jps

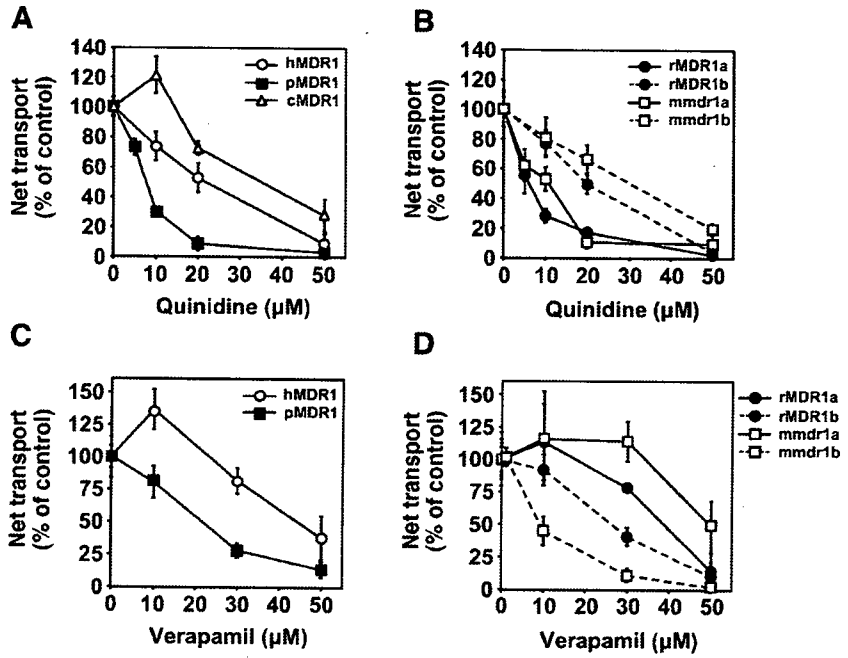

Figure 5. Concentration-dependent inhibition of the net transport of cyclosporin A by quinidine (A and B) and verapamil (C and D) at 3 h in *MDR1* transfected cells. (B and D) A solid line shows the MDR (mdr) 1a. A dotted line shows MDR (mdr) 1b. The concentration of cyclosporin A was 30.7 nM. Each point represents the mean ± SEM of three or more independent measurements.

be a more potent inhibitor than quinidine using a human *MDR1* transfected NIH3T3 cell line. To clarify the species differences in the inhibitory effects on daunorubicin transport via P-gp, the relative IC_{50} value, which is the IC_{50} value of quinidine divided by that of verapamil, was calculated. The relative IC_{50} values of mmdr1a (0.89) and cMDR1 (10.70) were 0.17- and 2.0-fold, respectively, compared to that of hMDR1 (5.25). This result clearly demonstrated the existence of species differences in the inhibitory effects on the P-gp-mediated daunorubicin transport among human, monkey, canine, rat, and mouse.

Second, using other typical P-gp substrates, digoxin and cyclosporin A, the IC_{50} values of

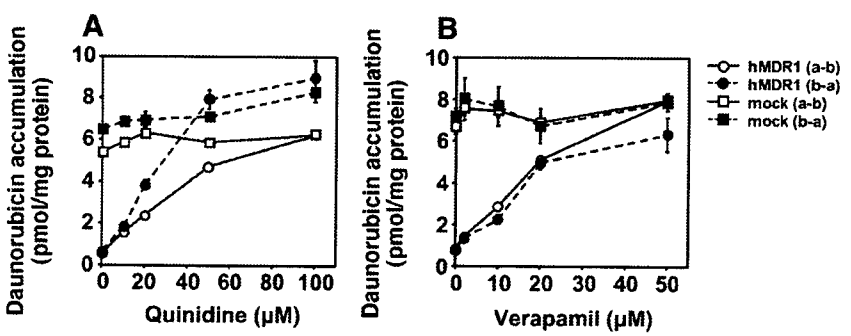

Figure 6. Intracellular accumulation in daunorubicin transport at 3 h in the presence or absence of quinidine (A) and verapamil (B) in hMDR1 and mock cells. The concentration of daunorubicin was 25.8 nM. The concentration of quinidine and verapamil ranged from 0 to 100 μM and 0 to 50 μM, respectively. Each point represents the mean ± SEM of three or more independent measurements.

quinidine and verapamil were determined to compare the inhibitory effect. For the digoxin transport, both quinidine and verapamil showed the same IC_{50} values in hMDR1. The inhibitory effect of quinidine and verapamil on the digoxin transport in hMDR1 was consistent with that of a previous result using Caco-2 cells.[17] Although verapamil was a more effective inhibitor than quinidine toward rMDR1a and rMDR1b in the present study, the effects on the renal tubular secretion of digoxin in isolated perfused rat kidney showed no differences between quinidine and verapamil.[18] The discrepancy may be caused by differences in the experimental system and/or the metabolism in rat kidney. The relative IC_{50} values of pMDR1, rMDR1a, rMDR1b, and mmdr1b cells were more than 2.00, while those of cMDR1 and mmdr1a were less than 1.00. For the cyclosporin A transport, only in mmdr1b was the inhibition of verapamil stronger than that of quinidine. Therefore, the species differences in the inhibitory effects on P-gp-mediated digoxin and cyclosporin A transport were quite obvious.

In the *MDR1* transfected cells, the intracellular accumulation of daunorubicin and cyclosporin A correlated with the concentration of the inhibitors, while that of digoxin did not change, which was consistent with our previous report.[19] The intracellular accumulation of digoxin was very low compared to those of daunorubicin and cyclosporin A, indicating that the intracellular accumulation might not be a suitable parameter to evaluate the inhibitory effects on P-gp-mediated drug transport.

It has been reported that human and mouse (encoded by *mdr1a* and *mdr1b*) P-gps have different capacities to confer resistance to colchicine and actionmycin D.[20] In our present data, hMDR1, mmdr1a, and mmdr1b showed different IC_{50} values for the inhibitors. However, hMDR1 and cMDR1 exhibited almost the same sensitivity to quinidine and hMDR1, pMDR1, and rMDR1a had almost the same sensitivity to verapamil. These results suggested that the inhibitory effects on P-gp-mediated drug transport were different depending on the inhibitors and the species. Species differences in the inhibitory effects of P-gp activity may be caused by differences in the amino acid residues in the drug-binding site of P-gp. Since the prazosin binding site has been reported to be the amino acid sequences 248-312, 758-800, and 1160-1218 for hamster P-gp[21] but 1135-1169 for human P-gp,[22] differences in the binding site may change the inhibitory effects. The information of the species differences is very restricted. Therefore, further investigations are needed to elucidate the mechanism responsible for such differences.

Mouse P-gps encoded by *mdr1a* and *mdr1b* possess different potencies in terms of the reversal effect in response to inhibitors.[20,23,24] In the present study, not only mmdr1a and mmdr1b but rMDR1a and rMDR1b showed different sensitivities to the P-gp inhibitors. It has been reported that the rat (encoded by *MDR1a* or *MDR1b*) and mouse (encoded by *mdr1a* and *mdr1b*) P-gp isoforms expressed tissue-specific patterns[25–27] and had different sensitivities to the P-gp inhibitors. Therefore, attention should be paid to their tissue-specific patterns and sensitivity to the P-gp inhibitors when drug interactions via P-gp in humans are to be predicted using *in vivo* and/or *in vitro* data obtained from the rodents. The present study was an *in vitro* study and the *in vitro* experimental condition may sometimes differ from the clinical situation. One of the problems is whether the *in vitro* concentrations of the substrate and the inhibitor could reflect on those in human *in vivo*. In the *in vitro* inhibition study using MDCKII-MDR1 and LLC-GA5-COL150 cells, an IC_{50} value of the inhibitor was μM whereas the substrate concentration was nM.[28,29] Therefore, the selected concentrations of the substrates and inhibitors in the present study were referred to the previous reports. The present study demonstrated that species differences in the inhibitory effects would exist in the same condition, suggesting that the inhibitory effects may differ among species in *in vivo* situations. In the present study, the IC_{50} values of the inhibitors on drug transports via P-gp from various species were firstly calculated and compared.

In conclusion, the present study revealed that species differences in the inhibitory effects on P-gp-mediated drug transport should not be disregarded among human, monkey, canine, rat, and mouse. The inhibitory effects on P-gp-mediated drug transport were different depending on the P-gp inhibitors. Experimental animals are useful tools, but they do not, in general, provide information that can be directly extrapolated to humans. Detailed information about species differences is needed when extrapolating animal data to human pharmacokinetics more precisely. We hope that the present study will provide useful information for predicting drug interactions mediated by P-gp.

DOI 10.1002/jps

ACKNOWLEDGMENTS

We acknowledge Mr. Brent Bell for reviewing the manuscript.

REFERENCES

1. Juliano RL, Ling V. 1976. A surface glycoprotein modulating drug permeability in Chinese hamster ovary cell mutants. Biochim Biophys Acta 455: 152–162.
2. Senior AE, Gadsby DC. 1997. ATP hydrolysis cycles and mechanism in P-glycoprotein and CFTR. Semin Cancer Biol 8:143–150.
3. Ambudkar SV, Dey S, Hrycyna CA, Ramachandra M, Pastan I, Gottesman MM. 1999. Biochemical, cellular, and pharmacological aspects of the multidrug transporter. Annu Rev Pharmacol Toxicol 39:361–398.
4. Tanigawara Y, Okamura N, Hirai M, Yasuhara M, Ueda K, Kioka N, Komano T, Hori R. 1992. Transport of digoxin by human P-glycoprotein expressed in a porcine kidney epithelial cell line (LLC-PK_1). J Phamacol Exp Ther 263:840–845.
5. Thiebaut F, Tsuruo T, Hamada H, Gottesman MM, Pastan I, Willingham MC. 1987. Cellular localization of the multidrug-resistance gene product P-glycoprotein in normal human tissues. Proc Natl Acad Sci USA 84:7735–7738.
6. Bussey HI. 1982. The influence of quinidine and other agents on digitalis glycosides. Am Heart J 104:289–302.
7. Verschraagen M, Koks CH, Schellens JH, Beijnen JH. 1999. P-glycoprotein system as a determinant of drug interactions: The case of digoxin-verapamil. Pharmacol Res 40:301–306.
8. Tsuji A. 2002. Transporter-mediated drug interactions. Drug Metab Pharmacokinet 17:253–274.
9. Katoh M, Suzuyama N, Takeuchi T, Yoshitomi S, Asahi S, Yokoi T. 2006. Kinetic analyses for species differences in P-glycoprotein-mediated drug transport. J Pharm Sci, in press.
10. Takeuchi T, Yoshitomi S, Higuchi T, Ikemoto K, Niwa S, Ebihara T, Katoh M, Yokoi T, Asahi S. 2006. Establishment and characterization of the transformants stably-expressing *MDR1* derived from various animal species in LLC-PK_1. Pharm Res 23:1460–1472.
11. Lowry OH, Rosebrough NJ, Farr AL, Randall RJ. 1951. Protein measurement with the Folin phenol reagent. J Biol Chem 193:265–275.
12. Lin JH, Yamazaki M. 2003. Role of P-glycoprotein in pharmacokinetics: Clinical implications. Clin Pharmacokinet 42:59–98.
13. Schinkel AH, Jonker JW. 2003. Mammalian drug efflux transporters of the ATP binding cassette (ABC) family: An overview. Adv Drug Deliv Rev 55:3–29.
14. Pedersen KE. 1985. Digoxin interactions. The influence of quinidine and verapamil on the pharmacokinetics and receptor binding of digitalis glycosides. Acta Med Scand Suppl 697:1–40.
15. Choo EF, Leake B, Wandel C, Imamura H, Wood AJ, Wilkinson GR, Kim RB. 2000. Pharmacological inhibition of P-glycoprotein transport enhances the distribution of HIV-1 protease inhibitors into brain and testes. Drug Metab Dispos 28:655–660.
16. Cardarelli CO, Aksentijevich I, Pastan I, Gottesman MM. 1995. Differential effects of P-glycoprotein inhibitors on NIH3T3 cells transfected with wild-type (G185) or mutant (V185) multidrug transporters. Cancer Res 55:1086–1091.
17. Balimane PV, Patel K, Marino A, Chong S. 2004. Utility of 96 well Caco-2 cell system for increased throughput of P-gp screening in drug discovery. Eur J Pharm Biopharm 58:99–105.
18. Hori R, Okamura N, Aiba T, Tanigawara Y. 1993. Role of P-glycoprotein in renal tubular secretion of digoxin in the isolated perfused rat kidney. J Pharmacol Exp Ther 266:1620–1625.
19. Katoh M, Nakajima M, Yamazaki H, Yokoi T. 2000. Inhibitory potencies of 1,4-dihydropyridine calcium antagonists to P-glycoprotein-mediated transport: Comparison with the effects on CYP3A4. Pharm Res 17:1189–1197.
20. Tang-Wai DF, Kajiji S, DiCapua F., de Graaf D, Roninson IB, Gros P. 1995. Human (*MDR1*) and mouse (*mdr1, mdr3*) P-glycoproteins can be distinguished by their respective drug resistance profiles and sensitivity to modulators. Biochemistry 34:32–39.
21. Isenberg B, Thole H, Tummler B, Demmer A. 2001. Identification and localization of three photobinding sites of iodoarylazidoprazosin in hamster P-glycoprotein. Eur J Biochem 268:2629–2634.
22. Ambudkar SV, Kimchi-Sarfaty C, Sauna ZE, Gottesman MM. 2003. P-glycoprotein: From genomics to mechanism. Oncogene 22:7468–7485.
23. Yang CP, Cohen D, Greenberger LM, Hsu SI, Horwitz SB. 1990. Differential transport properties of two *mdr* gene products are distinguished by progesterone. J Biol Chem 265:10282–10288.
24. Kajiji S, Dreslin JA, Grizzuti K., Gros P. 1994. Structurally distinct MDR modulators show specific patterns of reversal against P-glycoproteins bearing unique mutations at serine$^{939/941}$. Biochemistry 33:5041–5048.
25. Arceci RJ, Croop JM, Horwitz SB, Housman D. 1988. The gene encoding multidrug resistance is induced and expressed at high levels during pregnancy in the secretory epithelium of the uterus. Proc Natl Acad Sci USA 85:4350–4354.
26. Teeter LD, Estes M, Chan JY, Atassi H, Sell S, Becker FF, Kuo MT. 1993. Activation of distinct

multidrug-resistance (P-glycoprotein) genes during rat liver regeneration and hepatocarcinogenesis. Mol Carcinog 8:67–73.

27. Schinkel AH, Smit JJ, van Tellingen O, Beijnen JH, Wagenaar E, van Deemter L, Mol CA, van der Valk MA, Robanus-Maandag EC, te Riele HP, Berns AJ, Borst P. 1994. Disruption of the mouse *mdr1a* P-glycoprotein gene leads to a deficiency in the blood-brain barrier and to increased sensitivity to drugs. Cell 77:491–502.
28. Keogh JP, Kunta JR. 2006. Development, validation and utility of an in vitro technique for assessment of potential clinical drug-drug interactions involving P-glycoprotein. Eur J Pharm Sci 27:543–554.
29. Kakumoto M, Sakaeda T, Takara K, Nakamura T, Kita T, Yagami T, Kobayashi H, Okamura N, Okumura K. 2003. Effects of carvedilol on MDR1-mediated multidrug resistance: Comparison with verapamil. Cancer Sci 94:81–86.

DOI 10.1002/jps

0090-9556/07/3509-1679–1686$20.00
DRUG METABOLISM AND DISPOSITION
Vol. 35, No. 9
15909/3245788
Printed in U.S.A.

DMD 35:1679–1686, 2007

Stereoselective Glucuronidation of 5-(4′-Hydroxyphenyl)-5-phenylhydantoin by Human UDP-Glucuronosyltransferase (UGT) 1A1, UGT1A9, and UGT2B15: Effects of UGT-UGT Interactions

Miki Nakajima, Hiroyuki Yamanaka, Ryoichi Fujiwara, Miki Katoh, and Tsuyoshi Yokoi

Drug Metabolism and Toxicology, Division of Pharmaceutical Sciences, Graduate School of Medical Science, Kanazawa University, Kanazawa, Japan

Received March 26, 2007; accepted June 13, 2007

ABSTRACT:

5-(4′-Hydroxyphenyl)-5-phenylhydantoin (4′-HPPH), a major metabolite of phenytoin in human, is exclusively metabolized to a glucuronide. 4′-HPPH has a chiral center. (*S*)-4′-HPPH is a predominant form produced from phenytoin in humans, and (*R*)-4′-HPPH is an extremely toxic form with respect to gingival hyperplasia. In the present study, we investigated stereoselective 4′-HPPH *O*-glucuronide formation in human liver microsomes. Human liver microsomes predominantly formed (*S*)-4′-HPPH *O*-glucuronide rather than (*R*)-4′-HPPH *O*-glucuronide from racemic 4′-HPPH. Among human UDP-glucuronosyltransferase (UGT) enzymes, UGT1A1, UGT1A9, and UGT2B15 showed 4′-HPPH *O*-glucuronide formation. Interestingly, UGT1A1 stereoselectively formed (*R*)-4′-HPPH *O*-glucuronide, whereas UGT1A9 and UGT2B15 stereoselectively formed (*S*)-4′-HPPH *O*-glucuronide from racemic 4′-HPPH. By using UGT1A double-expression systems in HEK293 cells that we previously established, the effects of UGT-UGT interactions on 4′-HPPH *O*-glucuronide formation were investigated. It was demonstrated that coexpression of UGT1A4 increased the V_{max} values of (*S*)- and (*R*)-4′-HPPH *O*-glucuronide formation catalyzed by UGT1A1 but decreased the V_{max} values of (*S*)- and (*R*)-4′-HPPH *O*-glucuronide formation catalyzed by UGT1A9. Coexpression of UGT1A6 increased the S_{50} values and decreased the V_{max} values of (*S*)- and (*R*)-4′-HPPH glucuronide formation catalyzed by UGT1A1 and UGT1A9. However, the interaction did not alter the stereoselectivity. In conclusion, we found that 4′-HPPH *O*-glucuronide formation in human liver microsomes is catalyzed by UGT1A1, UGT1A9, and UGT2B15 in a stereoselective manner, being modulated by interaction with other UGT1A isoforms.

Phenytoin, 5,5-diphenylhydantoin, is a widely used anticonvulsant drug. It is metabolized to 5-(4′-hydroxyphenyl)-5-phenylhydantoin (4′-HPPH) mainly by cytochrome P450 CYP2C9 and, to a small extent, by CYP2C19 in humans (Giancarlo et al., 2001). 4′-HPPH has an asymmetric carbon atom. CYP2C9 preferentially catalyzes the formation of the (*S*)-enantiomer of 4′-HPPH, whereas CYP2C19 is not stereoselective (Bajpai et al., 1996; Yasumori et al., 1999). It has been reported that 98% of circulating 4′-HPPH after phenytoin administration is the (*S*)-enantiomer in humans (Ieiri et al., 1995; Yasumori et al., 1999). 4′-HPPH has no anticonvulsant properties, but it is associated with side effects such as gingival hyperplasia, somnolence, dry month, and general fatigue (Ieiri et al., 1992). The (*R*)-enantiomer, although it is a minor metabolite, has been reported to be extremely toxic with respect to gingival hyperplasia (Ieiri et al., 1995). A number of studies suggested that 4′-HPPH is bioactivated by peroxidase to a free radical intermediate, which can oxidize lipids, proteins, and DNA (Kim and Wells, 1996; Parman et al., 1998). However, 4′-HPPH is exclusively metabolized to glucuronide, which is a major metabolite of phenytoin in human (Yamanaka et al., 2005). Thus, glucuronidation is an important detoxification pathway of 4′-HPPH.

Glucuronidation of a variety of xenobiotics and endogenous compounds is catalyzed by UDP-glucuronosyltransferases (UGTs). In humans, the UGT superfamily of genes is divided into two families, *UGT1* and *UGT2*, based on sequence similarity at the amino acid level (Mackenzie et al., 2005). In our previous study, we found that 4′-HPPH *O*-glucuronide formation in human liver microsomes is catalyzed by UGT1A enzyme(s), although we could not determine which UGT1A enzymes make the major contribution (Nakajima et al., 2002). The limitation of the previous study was that the sensitivity was too low to detect the activity by recombinant UGTs. In our recent study, we improved the assay procedure and the HPLC condition to increase the sensitivity for the detection of 4′-HPPH *O*-glucuronide. Moreover, we could successfully separate the (*S*)- and (*R*)-4′-HPPH glucuronide in the improved HPLC condition. In the present study, we sought to determine the catalytic activities for the (*S*)- and (*R*)-4′-HPPH glucuronide formation by each human UGT enzyme. Recently, we reported that UGT1A enzymes interact with each other, possibly by heterodimerization, changing the kinetics of the enzymatic activity (Fujiwara et al., 2007a,b). Extending these studies, we investigated the effects of

H.Y. is supported as a Research Fellow of the Japan Society for the Promotion of Science.

Article, publication date, and citation information can be found at http://dmd.aspetjournals.org.

doi:10.1124/dmd.107.015909.

ABBREVIATIONS: 4′-HPPH, 5-(4′-hydroxyphenyl)-5-phenylhydantoin; UGT, UDP-glucuronosyltransferase; HPLC, high-performance liquid chromatography; UDPGA, UDP-glucuronic acid.

UGT-UGT interactions on the stereoselective formation of 4′-HPPH *O*-glucuronides.

Materials and Methods

Materials. 4′-HPPH, UDP-glucuronic acid (UDPGA), and alamethicin were purchased from Sigma-Aldrich (St. Louis, MO). Phenytoin was purchased from Wako Pure Chemicals (Osaka, Japan). Pooled human liver microsomes were from BD Gentest (Woburn, MA). Racemic 4′-HPPH was separated to (*S*)- and (*R*)-enantiomers according to a method of Yasumori et al. (1999) using a Chiralcel OJ column (4.6 × 250 mm, 10 μm; Daicel Chemical, Osaka, Japan). All other chemicals and solvents were of the highest grade commercially available.

Recombinant Human UGT and Immunoblot Analysis. Microsomes from baculovirus-infected insect cells expressing human UGT1A1, UGT1A3, UGT1A4, UGT1A6, UGT1A7, UGT1A8, UGT1A9, UGT1A10, UGT2B4, UGT2B7, UGT2B15, UGT2B17, and CYP2C9 (Supersomes) were from BD Gentest. Single- and double-expression systems of UGT1A1, UGT1A4, UGT1A6, and UGT1A9 stably expressed in HEK293 cells were previously established in our laboratory (Fujiwara et al., 2007a,b). For double-expression systems, the clones expressing two isoforms almost equally were selected in this study. Total cell homogenates were prepared as described previously (Fujiwara et al., 2007b). The expression levels of UGT1A proteins in the homogenates were determined by immunoblot analysis using rabbit anti-human UGT1A polyclonal antibody (BD Gentest) and were defined on the basis of a standard curve using the UGT1A1 single-expression system (1 unit/1 mg of cell homogenates), as described previously (Fujiwara et al., 2007b).

(*S*)- and (*R*)-4′-HPPH *O*-Glucuronide Formation. A typical incubation mixture (100 μl total volume) contained 50 mM Tris-HCl buffer (pH 7.4), 5 mM $MgCl_2$, 2.5 mM UDPGA, 25 μg/ml alamethicin, 0.5 mg/ml human liver microsomes or 1 mg/ml recombinant UGTs (single- or double-expression systems in HEK293 cells and Supersomes), and racemic 4′-HPPH or each enantiomer. Because it was confirmed that alamethicin increased 4′-HPPH *O*-glucuronide formation both in human liver microsomes (2.2- to 2.5-fold) and by recombinant UGTs (1.0- to 1.8-fold), alamethicin was included in all incubation mixtures. 4′-HPPH was dissolved in methanol, and the final concentration of the organic solvent in the incubation mixture was set at 1%. It was confirmed that the inhibitory effects of 1% methanol on 4′-HPPH *O*-glucuronidation were negligible. The reactions were initiated by the addition of UDPGA and were then incubated at 37°C for 60 min. The reactions were terminated by 100 μl of 10% perchloric acid. After the centrifugation at 10,000*g* for 5 min, the supernatant (50 μl) was injected into the HPLC system. HPLC analyses were performed using a PC-980 pump (Jasco, Tokyo, Japan), a UV-970 intelligent UV/visible detector (Jasco), an AS-950-10 autosampler (Jasco), a D-2500 integrator (Hitachi, Tokyo, Japan), and a CTO-6A column oven (Shimadzu, Kyoto, Japan) equipped with an YMC-Pack ODS-AM column (4.6 × 150 mm; 5 μm; YMC, Kyoto, Japan). The mobile phase was 10% acetonitrile-50 mM potassium dihydrogenphosphate. The flow rate was 0.7 ml/min, and the column temperature was 35°C. The eluent was monitored at

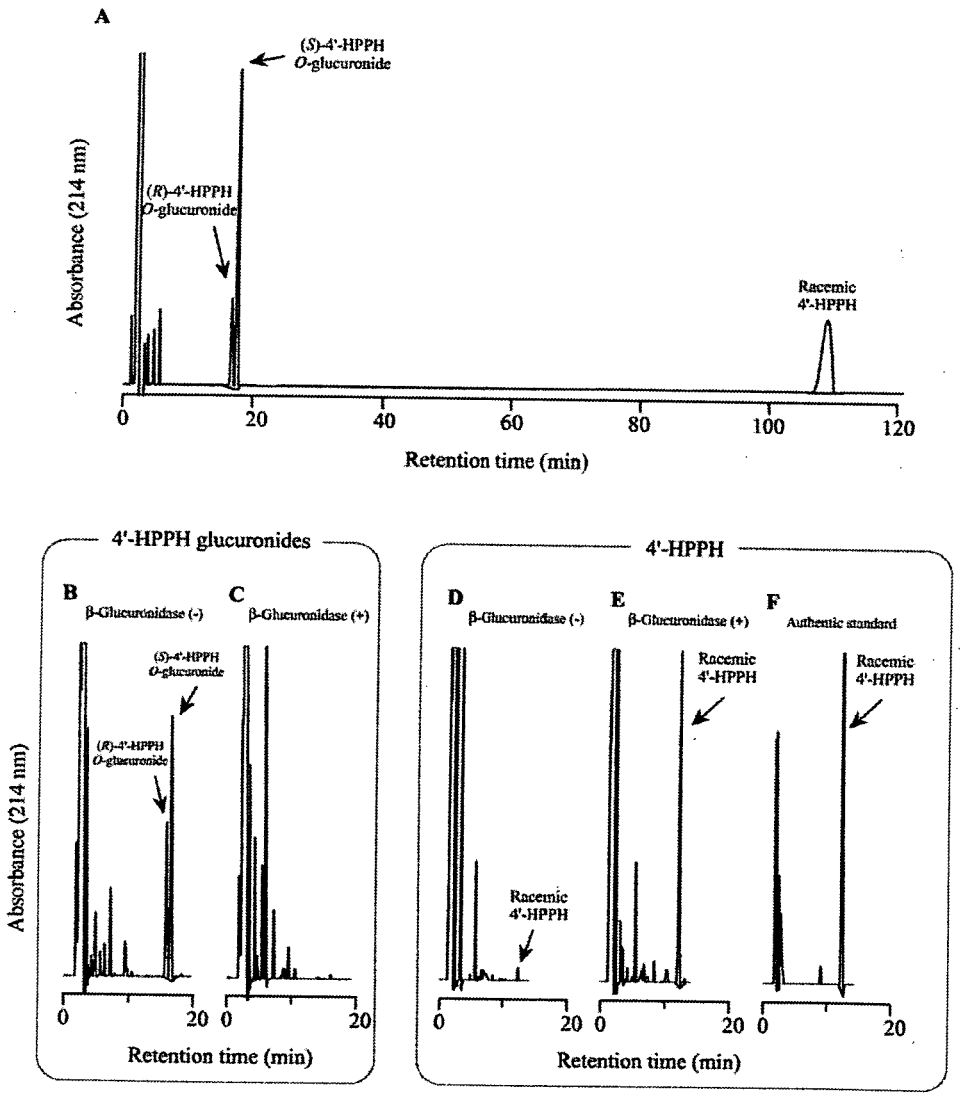

FIG. 1. Representative chromatogram of HPLC analysis of the (*S*)- and (*R*)-4′-HPPH *O*-glucuronide formation from racemic 4′-HPPH in human liver microsomes. Pooled human liver microsomes (0.5 mg/ml) were incubated with 100 μM racemic 4′-HPPH and 2.5 mM UDPGA at 37°C for 60 min (A). To quantify the 4′-HPPH *O*-glucuronides, the incubation mixtures with human liver microsomes including 4′-HPPH *O*-glucuronides were treated with β-glucuronidase. Chromatograms to detect the 4′-HPPH *O*-glucuronides in the mixture treated with (C) and without (B) the β-glucuronidase. Chromatograms to detect the 4′-HPPH in the mixture treated with (E) and without (D) the β-glucuronidase. Chromatogram of the authentic standard of racemic 4′-HPPH (F).

214 nm with a noise-base clean Uni-3 (Union, Gunma, Japan). The Uni-3 can reduce the noise by integrating the output and increase the signal 3-fold by differentiating the output and 5-fold by further amplification with an internal amplifier, resulting in a maximum 15-fold amplification of the signal. The retention times of (*R*)- and (*S*)-4′-HPPH *O*-glucuronides and racemic 4′-HPPH were 16.8, 17.6, and 109 min (Fig. 1A). The detection limit of (*S*)- and (*R*)-4′-HPPH *O*-glucuronides was 0.1 pmol.

Quantification of 4′-HPPH *O*-Glucuronides. The incubation mixtures with human liver microsomes including 4′-HPPH *O*-glucuronides were extracted with diethyl ether to exclude the large amount of unconjugated 4′-HPPH. Peak heights of the 4′-HPPH *O*-glucuronides in the residual water phase were determined with the HPLC condition described above (Fig. 1B). 4′-HPPH in the residual water phase was also quantified (Fig. 1D) by comparing it with the peak height of the authentic standard (Fig. 1F), using the modified HPLC condition (the mobile phase was 20% acetonitrile-50 mM potassium dihydrogenphosphate, and the flow rate was 1 ml/min). The retention time of 4′-HPPH was 13.0 min. A part of the water phase was incubated with 800 U/ml β-glucuronidase at 37°C for 24 h. 4′-HPPH formed by the hydration of glucuronides was quantified (Fig. 1E). Once we determined the peak height per known content of 4′-HPPH *O*-glucuronide, it was applied to the calculation of the 4′-HPPH *O*-glucuronide formed in the incubation mixtures.

Kinetic Analyses of (*S*)- and (*R*)-4′-HPPH Glucuronide Formation. 4′-HPPH glucuronide formation in human liver microsomes and recombinant UGTs was determined with 5 to 500 μM racemic 4′-HPPH. To measure the activity in human liver microsomes at 1 mM racemic 4′-HPPH, 2 μl of 50 mM substrate in methanol was added to 100 μl of the incubation mixture, resulting in a 2% methanol concentration. Therefore, the observed activity was corrected with the inhibition percentage [5% for (*S*)-4′-HPPH *O*-glucuronide formation and 12% for (*R*)-4′-HPPH *O*-glucuronide formation]. Kinetic parameters were estimated by fitting untransformed experimental data to the Hill equation using a KaleidaGraph computer program (Synergy Software, Reading, PA) designed for nonlinear regression analysis.

The Hill equation, which describes sigmoidal kinetics, is

$$V = \frac{V_{max} \times S^n}{S_{50}{}^n + S^n} \quad (1)$$

where V is the velocity of the reaction, S is the substrate concentration, V_{max} is the maximum velocity, S_{50} is the substrate concentration showing the half V_{max}, and n is the Hill coefficient. Maximum clearance (CL_{max}), which has been proposed as an appropriate parameter for sigmoid kinetic data instead of intrinsic clearance (Houston and Kenworthy, 2000; Uchaipichat et al., 2004), was calculated by the following equation:

$$CL_{max} = \frac{V_{max}}{S_{50}} \times \frac{(n-1)}{n(n-1)^{1/n}} \quad (2)$$

Data are expressed as means ± S.D. of three independent determinations.

Statistical Analyses. Statistical significances of the kinetic parameters were determined by analysis of variance followed by Dunnett's test. A value of $P < 0.05$ was considered statistically significant.

Results

(*S*)- and (*R*)-4′-HPPH *O*-Glucuronide Formation in Human Liver Microsomes. When the pooled human liver microsomes were incubated with racemic 4′-HPPH and UDPGA, two peaks with retention times of 16.8 and 17.6 min were observed (Fig. 1A). Both peaks appeared to correspond to 4′-HPPH *O*-glucuronide, because these peaks disappeared by treatment with β-glucuronidase. The formation of these glucuronides increased linearly with an incubation time up to 90 min and with a protein concentration up to 2 mg/ml. To identify which of the two peaks corresponds to (*S*)-4′-HPPH *O*-glucuronide, (*S*)-4′-HPPH prepared from the incubation of phenytoin with recombinant CYP2C9 and an NADPH-generating system was used as the substrate. Incubation of the prepared (*S*)-4′-HPPH with the human liver microsomes and UDPGA showed only a peak with the retention

TABLE 1

Quantification of 4′-HPPH O-glucuronide

Incubation mixtures (100 μl) with human liver microsomes and racemic 4′-HPPH (500 μM) or 4′-HPPH enantiomers (50 μM) were extracted with diethyl ether to exclude the large amount of unconjugated 4′-HPPH. The residual water phase was divided into two parts; one was incubated with β-glucuronidase at 37°C for 24 h, and the others were incubated without β-glucuronidase. After removal of protein, aliquots of the incubation mixtures were subjected to HPLC to determine the peak heights of 4′-HPPH *O*-glucuronides and content of 4′-HPPH. By comparing the decreased peak heights of 4′-HPPH *O*-glucuronides with the increased 4′-HPPH by the treatment of β-glucuronidase, the peak height per 1 pmol of 4′-HPPH *O*-glucuronide was determined.

Substrate	Volume of Analyte	Hydrolyze (−)				Hydrolyze (+)			HPPH Formed by Hydration of Glucuronides (C − B)	Peak Height of Glucuronide per 1 pmol A/(C − B)
		4′-HPPH *O*-Glucuronide		Sum of (*S*)- and (*R*)-Glucuronides (A)	4′-HPPH (B)	4′-HPPH *O*-Glucuronide		4′-HPPH (C)		
		(*S*)-Glucuronide	(*R*)-Glucuronide			(*S*)-Glucuronide	(*R*)-Glucuronide			
	μl	*height*			*pmol*	*height*		*pmol*		
Racemic 4′-HPPH (500 μM)	50	456,181	299,242	755,423	34.8	N.D.	N.D.	852.9	818.1	923
	25	223,114	145,859	368,973	11.3	N.D.	N.D.	424.8	413.4	892
	5	46,160	27,310	73,470	4.6	N.D.	N.D.	84.9	80.4	915
(*S*)-4′-HPPH (50 μM)	50	109,600	N.D.	109,600	5.6	N.D.	N.D.	138.4	132.8	825
(*R*)-4′-HPPH (50 μM)	50	N.D.	69,990	69,990	5.2	N.D.	N.D.	87.6	82.4	850
										881 ± 4 (mean ± S.D.)

ND, not detected.

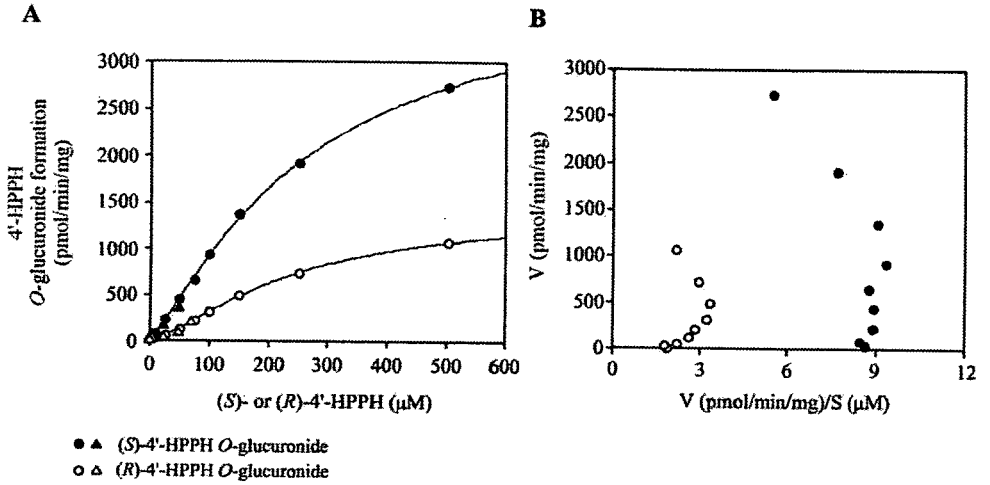

FIG. 2. Kinetic analyses of (*S*)- and (*R*)-4′-HPPH *O*-glucuronide formation in human liver microsomes. The substrate-velocity curve (A) and Eadie-Hofstee plot (B) of the 4′-HPPH *O*-glucuronide formation are shown. Pooled human liver microsomes were incubated with 5 μM to 1 mM racemic 4′-HPPH and 2.5 mM UDPGA at 37°C for 60 min. The abscissa denotes the concentrations of (*S*)- and (*R*)-4′-HPPH enantiomer, namely the half concentrations of racemic 4′-HPPH. ● and ○, (*S*)- and (*R*)-4′-HPPH *O*-glucuronide formation from racemic 4′-HPPH, respectively. ▲ and △, (*S*)- and (*R*)-4′-HPPH *O*-glucuronide formation from (*S*)- and (*R*)-4′-HPPH enantiomers, respectively. Since the quantity of 4′-HPPH enantiomers was limited, the activities could be measured only up to a 50 μM substrate concentration. Each data point represents the mean of three independent experiments.

time of 17.6 min. Accordingly, two peaks at 16.8 and 17.6 min were determined to correspond to (*R*)- and (*S*)-4′-HPPH *O*-glucuronides, respectively. For the quantification of the 4′-HPPH *O*-glucuronides, the decrease of 4′-HPPH *O*-glucuronides and the increase of 4′-HPPH were compared by the treatment of β-glucuronidase (Table 1). Repetitive estimations with an incubation mixture using racemic 4′-HPPH or each enantiomer as the substrate demonstrated that the peak height of 4′-HPPH *O*-glucuronide per 1 pmol was 881 ± 42 (coefficient of variation was 4.8%). These results suggest that the approach to quantify the 4′-HPPH *O*-glucuronides was sufficiently reliable.

Kinetic analyses of the (*S*)- and (*R*)-4′-HPPH *O*-glucuronide formation in the pooled human liver microsomes were performed with racemic 4′-HPPH. The kinetics was fitted to the Hill equations (Fig. 2). The abscissa denotes the concentrations of (*S*)- or (*R*)-4′-HPPH enantiomer, namely half concentrations of racemic 4′-HPPH. For (*S*)-4′-HPPH *O*-glucuronide formation, S_{50} was 256 ± 30 μM, V_{max} was 3.9 ± 0.2 nmol/min/mg, and the Hill coefficient was n = 1.3 ± 0.0. For the (*R*)-4′-HPPH *O*-glucuronide formation, S_{50} was 236 ± 17 μM, V_{max} was 1.4 ± 0.0 nmol/min/mg, and Hill coefficient was n = 1.5 ± 0.1. Thus, the CL_{max} of (*S*)-4′-HPPH *O*-glucuronide formation

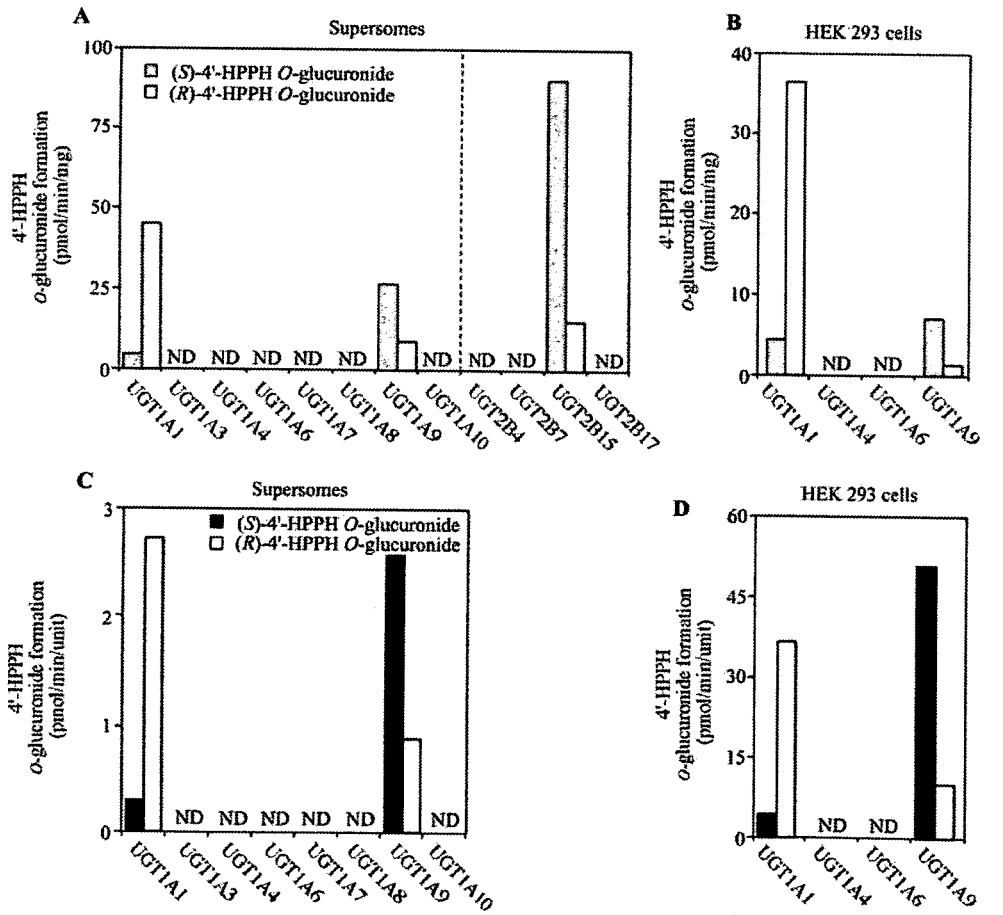

FIG. 3. (*S*)- and (*R*)-4′-HPPH *O*-glucuronide formation by recombinant human UGT enzymes expressed in baculovirus-infected insect cells (Supersomes) (A and C) or HEK293 cells (B and D). The activity was expressed as picomoles per minute per milligram (A and B) or picomoles per minute per unit (C and D). Each recombinant UGT (1 mg/ml) was incubated with 100 μM racemic 4′-HPPH and 2.5 mM UDPGA at 37°C for 60 min. ■ and □, (*S*)- and (*R*)-4′-HPPH *O*-glucuronide formation, respectively. Each column represents the mean of duplicate determinations. ND, not detected.

TABLE 2

Expression levels of each UGT1A protein in double-expression systems

Data are means ± S.D. (n = 3).

	UGT1A1	UGT1A4	UGT1A6	UGT1A9
		units/mg		
UGT1A1	1.00 ± 0.03			
UGT1A4		0.74 ± 0.01		
UGT1A6			0.09 ± 0.01	
UGT1A9				0.14 ± 0.02
UGT1A1/1A4	0.62 ± 0.02	0.62 ± 0.03		
UGT1A1/1A6	0.62 ± 0.03		0.69 ± 0.03	
UGT1A1/1A9	0.36 ± 0.01			0.26 ± 0.01
UGT1A4/1A9		0.29 ± 0.02		0.24 ± 0.02
UGT1A6/1A9			0.27 ± 0.01	0.30 ± 0.00

(2.3 ± 0.2 μl/min/mg) was 2.9-fold higher than that of (*R*)-4′-HPPH *O*-glucuronide formation (0.8 ± 0.1 μl/min/mg) in pooled human liver microsomes. To investigate whether one enantiomer affects the activity or the sigmoidal kinetics of the other, (*S*)- and (*R*)-4′-HPPH enantiomers were isolated from racemic 4′-HPPH. Although the activities could be measured only up to 50 μM concentrations of the (*S*)- and (*R*)-4′-HPPH enantiomers because of their limited quantity, they were almost the same as the activities with racemic 4′-HPPH at twice the concentration. Therefore, racemic 4′-HPPH was used as the substrate in the subsequent studies.

(*S*)- and (*R*)-4′-HPPH *O*-Glucuronide Formation by Recombinant UGT Enzymes. Recombinant human UGT enzymes expressed in baculovirus-infected insect cells were screened for 4′-HPPH *O*-glucuronide formation. As shown in Fig. 3A, UGT1A1, UGT1A9, and UGT2B15 showed 4′-HPPH *O*-glucuronide formation. UGT1A1 dominantly formed (*R*)-4′-HPPH *O*-glucuronide (43 pmol/min/mg) rather than (*S*)-4′-HPPH *O*-glucuronide (5 pmol/min/mg). In contrast, UGT1A9 and UGT2B15 dominantly formed (*S*)-4′-HPPH *O*-glucuronide (26 and 91 pmol/min/mg, respectively) rather than (*R*)-4′-HPPH *O*-glucuronide (9 and 15 pmol/min/mg, respectively). The HEK293 cell homogenates expressing human UGT1A1, UGT1A4, UGT1A6, and UGT1A9 were also used to determine the 4′-HPPH glucuronidation. UGT1A1 and UGT1A9 selectively formed (*R*)- and (*S*)-4′-HPPH *O*-glucuronides, respectively (Fig. 3B). To normalize the UGT1A expression levels, immunoblot analysis using anti-human UGT1A antibodies was performed. The expression levels of UGT1A1 and UGT1A9 in Supersomes were previously determined to be 15.9 and 10.4 units/mg, respectively (Fujiwara et al., 2007b). The expression levels of UGT1A1 and UGT1A9 in HEK293 expression systems were determined to be 1.00 ± 0.03 and 0.14 ± 0.02 unit/mg, respectively (Table 2). By the correction of the activity with the UGT1A expression level, the HEK293 expression systems showed higher activity than Supersomes (Fig. 3, C and D). In the HEK293 expression systems, (*S*)- and (*R*)-4′-HPPH *O*-glucuronide formation by UGT1A1 was 4 and 36 pmol/min/unit, respectively; the (*S*)- and (*R*)-4′-HPPH *O*-glucuronide formation by UGT1A9 was 51 and 10 pmol/min/unit, respectively.

Kinetics of (*S*)- and (*R*)-4′-HPPH *O*-Glucuronide Formation by Recombinant Human UGT Enzymes. Kinetic analyses of 4′-HPPH *O*-glucuronide formation by the UGT1A1, UGT1A9, and UGT2B15 Supersomes were performed with racemic 4′-HPPH. All of the kinetics was fitted to the Hill equation without (*R*)-4′-HPPH *O*-glucuronide formation by UGT1A9 (Table 3). UGT1A1 showed an S_{50} of 81 μM and V_{max} of 14 pmol/min/mg for (*S*)-4′-HPPH *O*-glucuronide formation and showed an S_{50} of 110 μM and V_{max} of 179 pmol/min/mg for (*R*)-4′-HPPH *O*-glucuronide formation. UGT1A9 showed an S_{50} of 25 μM and V_{max} of 38 pmol/min/mg for (*S*)-4′-HPPH *O*-glucuronide formation and showed an S_{50} of 33 μM and V_{max} of 16 pmol/min/mg for (*R*)-4′-HPPH *O*-glucuronide formation. UGT2B15 showed an S_{50} of 91 μM and V_{max} of 504 pmol/min/mg for (*S*)-4′-HPPH *O*-glucuronide formation and showed an S_{50} of 96 μM and V_{max} of 121 pmol/min/mg for (*R*)-4′-HPPH *O*-glucuronide formation.

Kinetics analyses of 4′-HPPH *O*-glucuronide formation by the recombinant UGT1A1 and UGT1A9 in HEK293 cells were also performed with racemic 4′-HPPH. The kinetics were fitted to the Hill equation (Fig. 4; Table 3). UGT1A1 showed an S_{50} of 48 μM and normalized V_{max} of 9 pmol/min/unit for (*S*)-4′-HPPH *O*-glucuronide formation and showed an S_{50} of 74 μM and normalized V_{max} of 110 pmol/min/unit for (*R*)-4′-HPPH *O*-glucuronide formation. UGT1A9 showed an S_{50} of 23 μM and normalized V_{max} of 67 pmol/min/unit for (*S*)-4′-HPPH *O*-glucuronide formation and showed an S_{50} of 56 μM and normalized V_{max} of 22 pmol/min/unit for (*R*)-4′-HPPH *O*-glucuronide formation.

Effects of Coexpression of Other UGT1A Isoforms on (*S*)- and (*R*)-4′-HPPH *O*-Glucuronide Formation Catalyzed by UGT1A1 or UGT1A9. Double-expression systems of human UGT1A in HEK293 cells were used to determine the effects of other isoforms on 4′-HPPH *O*-glucuronide formation catalyzed by UGT1A1 or

TABLE 3

Kinetic parameters of 4′-HPPH O-glucuronidation by recombinant human UGT enzymes

Data are means ± S.D. (n = 3).

	(*S*)-4′-HPPH *O*-Glucuronide Formation					(*R*)-4′-HPPH *O*-Glucuronide Formation				
	S_{50}	V_{max}	Normalized V_{max}	CL_{max}	n	S_{50}	V_{max}	Normalized V_{max}	CL_{max}	n
	μM	*pmol/min/mg*	*pmol/min/unit*	*nl/min/unit*		*μM*	*pmol/min/mg*	*pmol/min/unit*	*nl/min/unit*	
UGT1A1 Supersomes	81 ± 20	14 ± 1	1 ± 0	6 ± 1	1.4 ± 0.1	110 ± 27	179 ± 25	11 ± 2	55 ± 4	1.6 ± 0.3
UGT1A9 Supersomes	25 ± 1	38 ± 1	4 ± 0	91 ± 1	1.3 ± 0.0	33 ± 4	16 ± 1	2 ± 0	46 ± 3[a]	1.0 ± 0.1
UGT2B15 Supersomes	91 ± 12	504 ± 55	N.A.	N.A.	1.7 ± 0.1	96 ± 6	121 ± 19	N.A.	N.A.	2.2 ± 0.1
UGT1A1[b]	48 ± 5	9 ± 0	9 ± 0	23 ± 2	1.8 ± 0.2	74 ± 12	110 ± 5	110 ± 5	194 ± 20	1.6 ± 0.2
UGT1A1/1A4[b]	49 ± 1	7 ± 0	12 ± 0**	30 ± 1**	1.8 ± 0.2	70 ± 5	86 ± 3	138 ± 5**	250 ± 6**	1.7 ± 0.2
UGT1A1/1A6[b]	66 ± 2*	3 ± 0	4 ± 0**	10 ± 1**	1.7 ± 0.4	91 ± 14	35 ± 4	56 ± 6**	81 ± 6**	1.6 ± 0.2
UGT1A9[b]	23 ± 2	9 ± 1	67 ± 9	382 ± 16	1.5 ± 0.1	56 ± 14	3 ± 0	22 ± 3	56 ± 7	1.5 ± 0.4
UGT1A4/1A9[b]	22 ± 2	12 ± 2	52 ± 8	296 ± 28†	1.7 ± 0.1	41 ± 6	4 ± 1	15 ± 2†	50 ± 11	1.6 ± 0.2
UGT1A6/1A9[b]	35 ± 5††	15 ± 1	50 ± 4†	192 ± 18††	1.5 ± 0.1	54 ± 8	4 ± 1	14 ± 2†	35 ± 2†	1.5 ± 0.2

N.A., not available.
*$P < 0.005$.
**$P < 0.01$, compared with single-expression system of UGT1A1 in HEK293 cells.
†$P < 0.005$.
††$P < 0.01$, compared with single-expression system of UGT1A9 in HEK293 cells.
[a] The intrinsic clearance (V_{max}/K_m) was calculated, because the kinetics was fitted to Michaelis-Menten equation.
[b] HEK293 expression systems that were established in our previous studies (Fujiwara et al., 2007a,b).

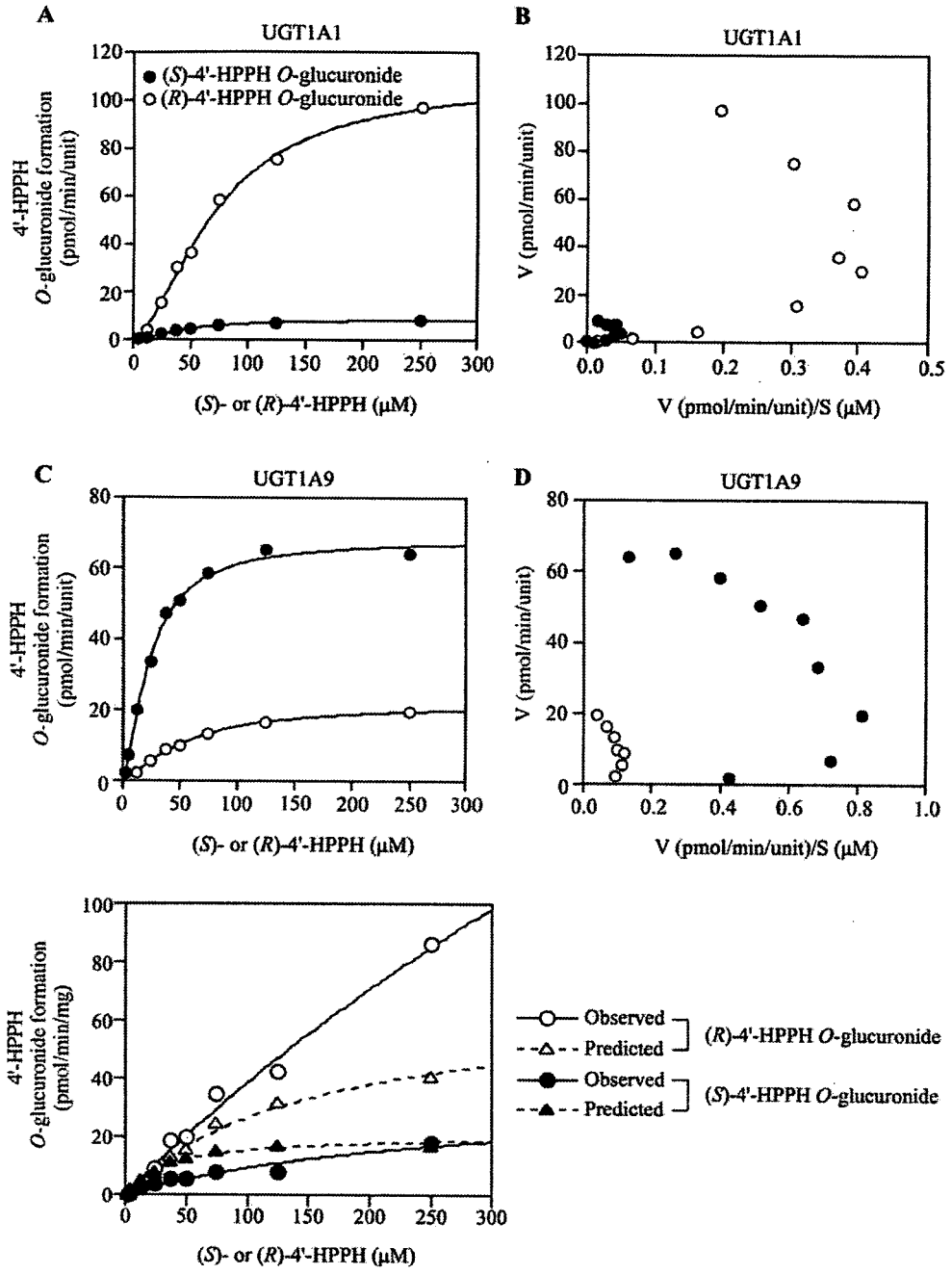

FIG. 4. Kinetic analyses of (*S*)- and (*R*)-4′-HPPH *O*-glucuronide formation by recombinant human UGT1A1 (A and B) and UGT1A9 (C and D) in HEK293 cells. The substrate-velocity curve (A and C) and Eadie-Hofstee plot (B and D) of the 4′-HPPH *O*-glucuronide formation are shown. Recombinant UGT1As (1 mg/ml) were incubated with racemic 4′-HPPH (5–500 μM) and 2.5 mM UDPGA at 37°C for 60 min. ● and ○, (*S*)- and (*R*)-4′-HPPH *O*-glucuronide formation, respectively. Each data point represents the mean of triplicate determinations.

FIG. 5. Kinetic analyses of (*S*)- and (*R*)-4′-HPPH *O*-glucuronide formation by a double-expression system of UGT1A1/UGT1A9. Recombinant UGT1As (1 mg/ml) were incubated with racemic 4′-HPPH (5–500 μM) and 2.5 mM UDPGA at 37°C for 60 min. Solid and dashed lines, observed and predicted activities; closed and open symbols, (*S*)- and (*R*)-4′-HPPH *O*-glucuronide formation, respectively. Each data point represents the mean of triplicate determinations.

UGT1A9. The activities of the double-expression systems were normalized with the expression levels of UGT1A1 and UGT1A9 proteins summarized in Table 1. Coexpression of UGT1A4 significantly increased the normalized V_{max} values of both (*S*)- and (*R*)-4′-HPPH *O*-glucuronide formation catalyzed by UGT1A1 (Table 3). Coexpression of UGT1A6 increased the S_{50} values and significantly decreased the normalized V_{max} values of both (*S*)- and (*R*)-4′-HPPH *O*-glucuronide formation-catalyzed UGT1A1. In contrast, coexpression of UGT1A4 decreased the normalized V_{max} values or both (*S*)- and (*R*)-4′-HPPH *O*-glucuronide formation catalyzed by UGT1A9. Coexpression of UGT1A6 significantly increased the S_{50} value and decreased the normalized V_{max} value of (*S*)-4′-HPPH *O*-glucuronide formation and decreased the normalized V_{max} value of (*R*)-4′-HPPH *O*-glucuronide formation catalyzed by UGT1A9. Thus, coexpression of UGT1A4 showed opposite effects toward UGT1A1- and UGT1A9-catalyzed 4′-HPPH *O*-glucuronide formation, but coexpression of UGT1A6 showed similar effects on UGT1A1- and UGT1A9-catalyzed 4′-HPPH *O*-glucuronide formation. In any case, the UGT-UGT interaction did not alter the stereoselectivity of the 4′-HPPH *O*-glucuronide formation.

The double-expression system UGT1A1/UGT1A9 was also used to investigate the interaction of UGT1A1 and UGT1A9 (Fig. 5). Because both isoforms have catalytic activity toward 4′-HPPH *O*-glucuronide formation, the activity by the double-expression system UGT1A1/UGT1A9 was predicted to be the sum of activities by UGT1A1 and UGT1A9. For (*S*)-4′-HPPH *O*-glucuronide formation, the observed activities were lower than the predicted activities based on the expression levels of UGT1A1 and UGT1A9 proteins (Fig. 5). In con-

trast, for (*R*)-4′-HPPH *O*-glucuronide formation, the observed activities were higher than the predicted activities at enantiomer concentrations >25 μM. These results suggested that (*R*)-4′-HPPH *O*-glucuronide formation catalyzed by UGT1A1 may be increased by the coexpression of UGT1A9, and (*S*)-4′-HPPH *O*-glucuronide formation catalyzed by UGT1A9 may conversely be decreased by the coexpression of UGT1A1.

Discussion

It has been demonstrated that some UGT enzymes stereoselectively catalyze glucuronidation (Court et al., 2002; Tougou et al., 2004; Bichlmaier et al., 2006; Sten et al., 2006). In the present study, we characterized different human UGT enzymes for glucuronide formation using racemic 4′-HPPH. We found that UGT1A1 dominantly formed (*R*)-4′-HPPH *O*-glucuronide, but UGT1A9 and UGT2B15 dominantly formed (*S*)-4′-HPPH *O*-glucuronide. In human liver microsomes, (*S*)-4′-HPPH *O*-glucuronide formation was predominant compared with (*R*)-4′-HPPH *O*-glucuronide formation. Which UGT isoform has a major contribution to the (*S*)- and (*R*)-4′-HPPH *O*-glucuronide formation in human liver microsomes? To address the issue, the absolute protein levels of each UGT isoform in human liver microsomes should be determined. Alternatively, specific substrates or inhibitors for each UGT isoform can be used to estimate the contribution quantitatively. Unfortunately, the lack of a methodology for the quantification of the absolute UGT protein levels beyond UGT1A and UGT2B subfamilies as well as a lack of specific substrates or inhibitors prevents us from accomplishing a quantitative estimation.

Concerning stereoselectivity, the question is raised whether the preference for the (*S*)- and (*R*)-enantiomers is determined by the binding affinity of substrates or by the rate of transfer of glucuronic acid to the already-bound substrate. Kinetic analyses for UGT1A1 and UGT2B15 activities revealed that the S_{50} values for the two enantiomers differed much less than the corresponding V_{max} values (Table 3). On this basis, it appears that the differences in the rate of glucuronic acid transfer to the aglycone are the major determinant of the stereoselectivity. In the case of UGT1A9, both differences in the rate of glucuronic acid transfer to the aglycone and in the affinity of the enzyme for 4′-HPPH enantiomers may be involved.

When the activities normalized with the UGT expression level were compared between two recombinant systems (Fig. 3), the activities by the recombinant UGT1A expressed in the baculovirus-infected insect cells were much lower (1/10-1/20) than those by recombinant UGT1A expressed in HEK293 cells. The phenomenon was not specific for 4′-HPPH *O*-glucuronide formation, because similar results were obtained with other substrates such as estradiol, serotonin, and propofol (data not shown). The differences between the recombinant systems might be due to differences in the membrane environment or lipid components in the host cells. Furthermore, the differences in the post-translational modulation of UGT such as glycosylation or phosphorylation between the insect cells and HEK293 cells might be responsible, as such modulations have been reported to affect the UGT activity (Barbier et al., 2000; Basu et al., 2005).

It has been reported that UGTs form homo- and heterodimers or oligomers (Matern et al., 1982; Meech and Mackenzie, 1997; Ghosh et al., 2001; Kurkela et al., 2003). In our recent studies (Fujiwara et al., 2007a,b), the glucuronidations of a variety of typical substrates were determined using the double-expression systems of human UGT1A enzymes to investigate the effects of the heterodimerization on the enzymatic activity. These previous studies demonstrated that coexpression of other UGT1A isoforms differently changed the kinetics of specific activities depending on the substrates as well as the UGT isoforms. Extending our studies, we found that the coexpression of UGT1A4 and UGT1A6 differently affected the kinetics of 4′-HPPH *O*-glucuronide formation by UGT1A1 or UGT1A9. Thus, the UGT-UGT interactions, which may also occur in human liver microsomes, affected the kinetics of 4′-HPPH *O*-glucuronide formation. The kinetic analyses revealed sigmoid curves in both (*S*)- and (*R*)-4′-HPPH *O*-glucuronide formation by recombinant UGT1A1 and UGT1A9. The sigmoid curve may indicate positive cooperativity owing to the binding of multiple substrate molecules to a single enzyme active site or to the existence of multiple conformations of the enzyme (Cornish-Bowden, 1995). In particular, allosteric effects would be feasible, because UGT forms a dimer or oligomer. It is interesting that the cooperativity was not affected by the coexpression of other isoforms, possibly heterodimerization. The S_{50} values of (*S*)- and (*R*)-4′-HPPH *O*-glucuronide formation in human liver microsomes were unexpectedly higher than those by recombinant UGT enzymes. Although the coexpression of other isoforms substantially increased the K_m values for certain substrates (Fujiwara et al., 2007a,b), prominent effects on the S_{50} values were not observed in the case of 4′-HPPH. We are also interested in interactions between UGT1A and UGT2B. Double-expression systems of UGT1A and UGT2B isoforms are now being constructed in our laboratory to investigate the effects of the interaction on the enzymatic activity. In addition, the possibility that other enzymes such as cytochrome P450 might also interact with UGT1A to affect the kinetics cannot be excluded. Further studies will be worth pursuing.

In the present study, we characterized the stereoselective 4′-HPPH *O*-glucuronide formation by human UGT1A1, UGT1A9, and UGT2B15. Furthermore, it was demonstrated that interaction between UGT1A enzymes differently affected the kinetics of (*S*)- and (*R*)-4′-HPPH *O*-glucuronide formation catalyzed by UGT1A1 and UGT1A9 but did not affect the stereoselectivity.

Acknowledgments. We acknowledge Brent Bell for reviewing the manuscript.

References

Bajpai M, Roskos LK, Shen DD, and Levy RH (1996) Roles of cytochrome P4502C9 and cytochrome P4502C19 in the stereoselective metabolism of phenytoin to its major metabolites. *Drug Metab Dispos* **24**:1401–1403.

Barbier O, Girard C, Breton R, Belanger A, and Hum DW (2000) *N*-Glycosylation and residue 96 are involved in the functional properties of UDP-glucuronosyltransferase enzymes. *Biochemistry* **39**:11540–11552.

Basu NK, Kovarova M, Garza A, Kubota S, Saha T, Mitra PS, Banerjee R, Rivera J, and Owens IS (2005) Phosphorylation of a UDP-glucuronosyltransferase regulates substrate specificity. *Proc Natl Acad Sci U S A* **102**:6285–6290.

Bichlmaier I, Siiskonen A, Finel M, and Yli-Kauhaluoma J (2006) Stereochemical sensitivity of the human UDP-glucuronosyltransferases 2B7 and 2B17. *J Med Chem* **49**:1818–1827.

Cornish-Bowden A (1995) *Fundamentals of Enzyme Kinetics*, rev ed, Portland Press, London.

Court MH, Duan SX, Guillemette C, Journault K, Krishnaswamy S, von Moltke LL, and Greenblatt DJ (2002) Stereoselective conjugation of oxazepam by human UDP-glucuronosyltransferases (UGTs): *S*-oxazepam is glucuronidated by UGT2B15, while *R*-oxazepam is glucuronidated by UGT2B7 and UGT1A9. *Drug Metab Dispos* **30**:1257–1265.

Fujiwara R, Nakajima M, Yamanaka H, Katoh M, and Yokoi T (2007a) Interactions between human UGT1A1, UGT1A4, and UGT1A6 affect their enzymatic activities. *Drug Metab Dispos*, in press.

Fujiwara R, Nakajima M, Yamanaka H, Nakamura A, Katoh M, Ikushiro S, Sakaki T, and Yokoi T (2007b) Effects of coexpression of UGT1A9 on enzymatic activities of human UGT1A isoforms. *Drug Metab Dispos* **35**:747–757.

Ghosh SS, Sappal BS, Kalpana GV, Lee SW, Chowdhury JR, and Chowdhury NR (2001) Homodimerization of human bilirubin-uridine-diphosphoglucuronate glucuronosyltransferase-1 (UGT1A1) and its functional implications. *J Biol Chem* **276**:42108–42115.

Giancarlo GM, Venkatakrishnan K, Granda BW, von Moltke LL, and Greenblatt DJ (2001) Relative contributions of CYP2C9 and 2C19 to phenytoin 4-hydroxylation in vitro: inhibition by sulfaphenazole, omeprazole, and ticlopidine. *Eur J Clin Pharmacol* **57**:31–36.

Houston JB and Kenworthy KE (2000) In vitro-in vivo scaling of CYP kinetic data not consistent with the classical Michaelis-Menten model. *Drug Metab Dispos* **28**:246–254.

Ieiri I, Goto W, Hirata K, Toshitani A, Imayama S, Ohyama Y, Yamada H, Ohtsubo K, and Higuchi S (1995) Effect of 5-(*p*-hydroxyphenyl)-5-phenylhydantoin (*p*-HPPH) enantiomers, major metabolites of phenytoin, on the occurrence of chronic-gingival hyperplasia: *in vivo* and *in vitro* study. *Eur J Clin Pharmacol* **49**:51–56.

Ieiri I, Hirata K, Higuchi S, Kojima K, Ikeda M, Yamada H, and Aoyama T (1992) Pharmaco-

epidemiological study on adverse reactions of antiepileptic drugs. *Chem Pharm Bull* **40**:1280–1288.

Kim PM and Wells PM (1996) Phenytoin-initiated hydroxyl radical formation: characterization by enhanced salicylate hydroxylation. *Mol Pharmacol* **49**:172–181.

Kurkela M, Garcia-Horsman JA, Luukkanen L, Morsky S, Taskinen J, Baumann M, Kostiainen R, Hirvonen J, and Finel M (2003) Expression and characterization of recombinant human UDP-glucuronosyltransferases (UGTs): UGT1A9 is more resistant to detergent inhibition than the other UGTs and was purified as an active dimeric enzyme. *J Biol Chem* **278**:3536–3544.

Mackenzie PI, Walter Bock K, Burchell B, Guillemette C, Ikushiro S, Iyanagi T, Miners JO, Owens IS, and Nebert DW (2005) Nomenclature update for the mammalian UDP glycosyltransferase (*UGT*) gene superfamily. *Pharmacogenet Genomics* **15**:677–685.

Matern H, Matern S, and Gerok W (1982) Isolation and characterization of rat liver microsomal UDP-glucuronosyltransferase activity toward chenodeoxycholic acid and testosterone as a single form of enzyme. *J Biol Chem* **257**:7422–7429.

Meech R and Mackenzie PI (1997) UDP-glucuronosyltransferase, the role of the amino terminus in dimerization. *J Biol Chem* **272**:26913–26917.

Nakajima M, Sakata N, Ohashi N, Kume T, and Yokoi T (2002) Involvement of multiple UDP-glucuronosyltransferase 1A isoforms in glucuronidation of 5-(4′-hydroxyphenyl)-5-phenylhydantoin in human liver microsomes. *Drug Metab Dispos* **30**:1250–1256.

Parman T, Chen G, and Wells PG (1998) Free radical intermediates of phenytoin and related teratogens. *J Biol Chem* **273**:25079–25088.

Sten T, Qvisen S, Uutela P, Luukkanen L, Kostiainen R, and Finel M (2006) Prominent but reverse stereoselectivity in propranolol glucuronidation by human UDP-glucuronosyltransferases 1A9 and 1A10. *Drug Metab Dispos* **34**:1488–1494.

Tougou K, Gotou H, Ohno Y, and Nakamura A (2004) Stereoselective glucuronidation and hydroxylation of etodolac by UGT1A9 and CYP2C9 in man. *Xenobiotica* **34**:449–461.

Uchaipichat V, Mackenzie PI, Guo XH, Gardner-Stephen D, Galetin A, Houston JB, and Miners JO (2004) Human UDP-glucuronosyltransferases: isoform selectivity and kinetics of 4-methylumbelliferone and 1-naphthol glucuronidation, effects of organic solvents, and inhibition by diclofenac and probenecid. *Drug Metab Dispos* **32**:413–423.

Yamanaka H, Nakajima M, Hara Y, Katoh M, Tachibana O, Yamashita J, and Yokoi T (2005) Urinary excretion of phenytoin metabolites, 5-(4′-hydroxyphenyl)-5-phenylhydantoin and its *O*-glucuronide in humans and analysis of genetic polymorphisms of UDP-glucuronosyltransferases. *Drug Metab Pharmacokinet* **20**:135–143.

Yasumori T, Chen LS, Li QH, Ueda M, Tsuzuki T, Goldstein JA, Kato R, and Yamazoe Y (1999) Human CYP2C-mediated stereoselective phenytoin hydroxylation in Japanese: difference in chiral preference of CYP2C9 and CYP2C19. *Biochem Pharmacol* **57**:1297–1303.

Address correspondence to: Dr. Tsuyoshi Yokoi, Drug Metabolism and Toxicology, Division of Pharmaceutical Sciences, Graduate School of Medical Science, Kanazawa University, Kakuma-machi, Kanazawa 920-1192, Japan.